

Hüseyin Onur Dönmez  
Hakan Tunçdemir

*Original Research*

**Estimating support pressure with finite element and convergence-confinement method for different rock masses**

Amine Soufi  
Youssef Zerradi  
Mohammed Souissi  
Latifa Ouadif  
Anas Bahi

*Original Research*

**Enhancing the bearing capacity of friction anchor bolts through cementitious concrete injection for reinforced support in Imiter underground rock masses**

Serkan Çayırılı  
Hasan Serkan Gökçen  
Nuri Yüce  
Obaidullah Elchi

*Original Research*

**Utilization of wastes/by-products as grinding additives**

Leng Wu  
Ziling Song

*Original Research*

**Dust pollution characteristics and control measures of open cut coal mines**

Sair Kahraman  
Masoud Rostami  
Behnaz Dibavar

*Original Research*

**Evaluating machine utilization times for roadheaders used in coal mines: Multiple regression and artificial neural network analyses**



## **Scientific Mining Journal**

Vol: 62, No: 3, September, 2023

A peer-reviewed quarterly journal of the Chamber of Mining Engineers of Türkiye

### ***Editor-in-Chief***

Dr. A. Hakan Benzer, Hacettepe University

### ***Editors***

Dr. Hakan Başarır, Norwegian University of Science and Technology

Dr. Hakan Dündar, Hacettepe University

Dr. Güneş Ertunç, Hacettepe University

Dr. Sedat Esen, Esen Mining

Dr. Murat Kademli, Hacettepe University

Dr. Mehmet Kızıl, Queensland University

Dr. Ece Kundak, Eskişehir Osmangazi University

Dr. Abdullah Obut, Hacettepe University

Dr. Ümit Özer, Istanbul University - Cerrahpaşa

Dr. Oktay Şahbaz, Dumlupınar University

### ***Editor Assistants***

Sena Naz Gökdemir

Melis Orakcı

## **AIMS AND SCOPE**

*Scientific Mining Journal, which is published in open access electronic environment and in printed, is a periodical scientific journal of Union of Chambers of Turkish Engineers and Architects Chamber of Mining Engineers. The name of the journal was "Mining" until June 2016 and it has been changed to "Scientific Mining Journal" since September 2016 because it can be confused with popular journals with similar names and the ISSN number has been updated from 0024-9416 to 2564-7024. Scientific Mining Journal, published four times a year (March-June-September-December), aims to disseminate original scientific studies which are conducted according to the scientific norms and publication ethics at national and international scale, to scientists, mining engineers, the public; and thus to share scientific knowledge with society. The journal is in English. The journal covers theoretical, experimental, and applied research articles, which reflects the findings and results of an original research in the field of mining engineering; review articles, which assess, evaluates, and interprets the findings of a comprehensive review of sufficient number of scientific articles and summarize them at present information and technology level; technical notes, which may be defined as a short article that describes a novel methodology or technique; a case studies, which are based on the theoretical or real professional practice and involves systematic data collection and analysis. The journal gives priority to works that will enable the advancement of current available information necessary to serve humanity with nonrenewable mineral resources with the perspective of sustainable mining principles. In this context, mine exploration, mineral resource modeling, surveying, mine economics and feasibility, geostatistics, rock mechanics and geotechnics, diggability studies, underground and surface mining, mine design, support design in underground mines and tunnels, rock penetration and rock fragmentation, mine production planning and pit optimization, mine health and safety management, mine ventilation, methane emission and drainage in underground coal mines, mineral processing and beneficiation, process mineralogy, analytical techniques, mineral comminution, mineral classification and separation, flotation/flocculation, solid/liquid separation, physical enrichment methods, hydro and biometallurgy, production metallurgy, modeling and simulation, instrumentation and process control, recycling and waste processing, mining law, environmental health and management, transportation, machinery and equipment selection and planning, coal gasification, marble technology, industrial minerals, space mining, submarine mining and mechanization are included in the journal content. Submitted manuscripts are evaluated by the editorial board and expert referees independently in accordance with the best practices in academic publishing. The publishing rights of the manuscripts, approved for publication at the end of the evaluation process, are transferred to the Chamber of Mining Engineers by the authors.*

### **Scientific Mining Journal**

*Scientific Mining Journal is indexed or abstracted in:*

SCOPUS

Google Scholar

ULAKBİM TR Dizin

GeoRef

OpenAIRE

*Author Instructions, Editorial Advisory Board, the Peer Review Process and Reviewer Lists can be accessed from <http://www.mining.org.tr>*

### **Publication Ethics**

*Complying with the research and publication ethics is considered an indisputable precondition to be published. Publication Ethics can be accessed from <http://www.mining.org.tr>*

**Scientific Mining Journal**

*Owner on behalf of the Chamber of Mining Engineers of Türkiye: Ayhan Yüksel*

*Responsible editing manager: Mehmet Erşat Akyazılı*

*Correspondence address:  
Kültür mah, Yüksel Cd. No:40, 06420 Çankaya/Ankara*

*Tel: +90 312 425 10 80 / +90 312 418 36 57 • Fax: +90 312 417 52 90*

*e-mail: [smj@maden.org.tr](mailto:smj@maden.org.tr)  
web: <http://www.mining.org.tr>*

*Publication type: Local periodical, quarterly*

*Design: Sinem Deniz Kılıç*

*Printed at: Ziraat Gurup Matbaacılık Ambalaj San. ve Tic. A.Ş.*

*Printing date: 20.10.2023*

## CONTENTS

- Hüseyin Onur Dönmez  
Hakan Tunçdemir 99 *Original Research*  
**Estimating support pressure with finite element and convergence-confinement method for different rock masses**
- Amine Soufi  
Youssef Zerradi  
Mohammed Souissi  
Latifa Ouadif  
Anas Bahi 109 *Original Research*  
**Enhancing the bearing capacity of friction anchor bolts through cementitious concrete injection for reinforced support in Imiter underground rock masses**
- Serkan Çayırılı  
Hasan Serkan Gökçen  
Nuri Yüce  
Obaidullah Elchi 123 *Original Research*  
**Utilization of wastes/by-products as grinding additives**
- Leng Wu  
Ziling Song 131 *Original Research*  
**Dust pollution characteristics and control measures of open cut coal mines**
- Sair Kahraman  
Masoud Rostami  
Behnaz Dibavar 141 *Original Research*  
**Evaluating machine utilization times for roadheaders used in coal mines: Multiple regression and artificial neural network analyses**







## Estimating support pressure with finite element and convergence-confinement method for different rock masses

Hüseyin Onur Dönmez<sup>a,\*</sup>, Hakan Tunçdemir<sup>a,\*\*</sup>

<sup>a</sup> Istanbul Technical University, Faculty of Mines, Mining Engineering Department, Istanbul, TÜRKİYE

Received: 6 September 2023 \* Accepted: 3 October 2023

### ABSTRACT

Support pressure is a key factor in the stability of the excavation area during mining and tunneling. The vital thing desired in an underground engineering structure is to ensure that the structure survives safely throughout its lifetime. For this reason, choosing the right support system at the planning stage is very important for the pressure that will affect the support system must be determined with a certain convergence. This article aims to discuss the support pressures by the finite element method and convergence-confinement method and compare the results. A series of two-dimensional finite element models are established to analyze support pressure with different rock masses selected from the literature. The results reveal that the convergence-confinement method and the finite element method have high-order relationships regarding support pressures and displacements for weak rock masses. Therefore, it shows that support pressures and displacement values for similar conditions can be estimated by the convergence-confinement method, which is more practical than the finite element method.

**Keywords:** Support pressure, Finite element method, Convergence-confinement method, Underground mining, Tunneling

### Introduction

Today, the increasing population and urbanization rate cause people to live in large masses in limited areas. This situation brings with it some problems. Areas on earth are becoming increasingly inadequate and negatively affect people's living standards. Transportation is one of these negatively affected living standards. For this reason, road and railway tunnels are of great importance for safer and more comfortable transportation. At the same time, production amounts are increasing to meet the needs of the increasing population. Our underground resources, which are our most important source of raw materials, are scarce resources by nature, so the production levels are getting deeper. This causes underground mining to become more widespread and work at deeper levels. These two cases show that the need for underground structures is extremely high and increasing.

The main issue sought in an underground

structure is to ensure that the structure survives safely throughout its lifetime. Thus, choosing the right support system at the planning stage is significant.

To select and dimension the correct support system, first of all, the pressures that will affect the support system must be revealed with a certain convergence.

Theories for the estimation of support pressure began to emerge in the early 20th century (Protodyakonov, 1907). Theories started with the engineers working in this field converting their experiences into numerical data and equations and then continued with the classification of the different environments studied and the estimation of the support pressure by making use of them (Terzaghi, et al., 1946; Lauffer, 1958; Deere, 1964; Deere et al., 1970; Wickham et al., 1972; Bieniawski, 1973; Barton et al., 1974; Rose, 1982; Stille et al., 1982; Birön and Arıoğlu, 1985; Ünal and Özkan,

\*Corresponding author: donmezhu@itu.edu.tr • <https://orcid.org/0000-0002-5567-0824>

\*\*tdemir@itu.edu.tr • <https://orcid.org/0000-0001-9244-6728>

<https://doi.org/10.30797/madencilik.1356042>

1990; Goel et al., 1995; Palmstrom, 1995; Goel et al., 1996; Hoek and Brown, 1997; Singh et al., 1997; Palmstrom, 2000; Aydan et al., 2014).

The finite element method (FEM), which was first used in the aerospace industry in the 1960s and quickly found use in every branch of engineering, was also applied to underground structures and is a good tool for analyzing the support pressure of mine galleries and tunnels. Therefore, many researchers have been using FEM in their analysis (Seshagiri Rao, 2020; Sharma et al., 2020; Taghizadeh et al., 2020; Aygar, 2022; Huang, et al., 2022; Zhang et al., 2022; Cui et al., 2023; Kumar and Sahoo, 2023; Niu et al., 2023).

The convergence-confinement method (CCM) is an analytical tool for estimating the support pressure and displacements in a tunnel by applying a hypothetical pressure to the tunnel wall. The basic components of the CCM are the ground reaction curve (GRC), the longitudinal displacement profile (LDP) of the tunnel walls, and the support reaction curve (SRC) (Panet et al., 2001).

This study presents a numerical analysis of the support pressure estimation of the tunnels bored for 3 different rock masses selected from the literature as weak, medium, and good. 2D finite element software named RS2 (Rocscience, 2020a) was used to perform FEM, and RocSupport (Rocscience, 2020b) was used to perform CCM. Analyses with FEM were made for a horseshoe section tunnel or

gallery. However, CCM only allows the modeling of full circular cross-section openings. For this reason, in order to avoid any problem in the comparison of the models created, the circular cross-section tunnels with the same opening as used in the CCM model were remodeled in FEM for the same rock masses. A total of 591 points in 9 models were analyzed and the results of two different analysis methods were examined. Finally, this paper discusses the estimation of support pressures for different rock masses.

## 1. Materials and Methods

### 1.1. Analyzed Rock Masses

The geomechanical parameters given in Table 1 are from the Yacambú Quibor tunnel in Venezuela for the weak rock mass (Hoek, 2000), the underground power room in the Nathpa Jhakri Hydropower project in India for the medium rock mass (Jalote et al., 1996), and the power station tunnels in Argentina for the good rock mass (Moretto et al., 1993). The reason for using the data obtained from these studies is that they are also referenced by the RS2 software due to their high representation power of the rock masses in which they are located (Hoek, 2000).

The tunnel shape and dimensions chosen are in the form of a horseshoe, 5x5 m in size, which is given in Figure 1, which is the most frequently used in mine galleries in Turkey.

**Table 1.** Geomechanical parameters of different rock masses used in the analyses (Hoek, 2000)

Parameters		Weak	Medium	Good
Intact rock strength (MPa)	$\sigma_{ci}$	50	30	110
Geological Strength Index	GSI	25	65	75
Hoek-Brown constant	$m_i$	10	15	28
Hoek-Brown constant	$m_b$	0.481	4.3	11.46
Hoek-Brown constant	s	0.0002	0.02	0.062
Constant	a	0.53	0.5	0.501
Deformation modulus (MPa)	$E_m$	1000	10000	45000

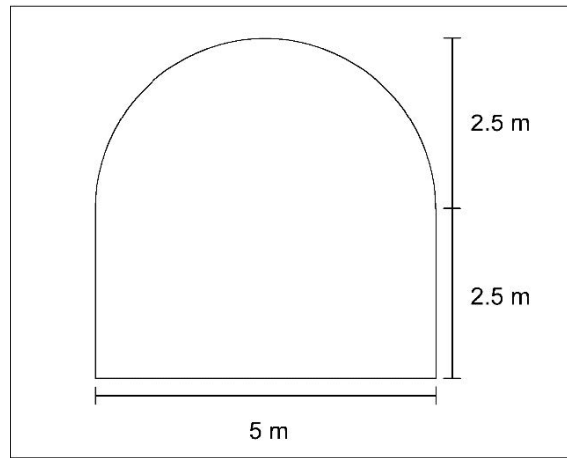


**Figure 1.** Shape and dimensions of the analyzed tunnel

### 1.2. Convergence-Confinement Method

The convergence-confinement approach developed by Panet and Guellec in 1974 is frequently used to evaluate tunnel wall deformations and offer recommendations for the design of rock supports (Brown et al., 1983; Carranza-Torres and Fairhurst, 2000; Panet and Sulem, 2022).

According to Figure 2, a circular tunnel with hydrostatic field stresses is excavated in an isotropic material, and the plane strain requirement is satisfied by the stress condition at a cross-section suffi-

ciently removed from the tunnel face (for instance, section B-B). The pressure that rock supports carry when they are positioned behind the tunnel face is less than the initial pressure  $p_0$  and they do not carry the complete support load from the rock mass. This is brought on by the tunnel face's supportive role in carrying some of the loads of the rock mass. The support from the face effect is represented by a fictitious internal pressure  $p_i$ . With the advancement of the tunnel face, the radial displacement on the walls increases as the face effect  $p_i$  on the section under study decreases (Wang and Cai, 2022).

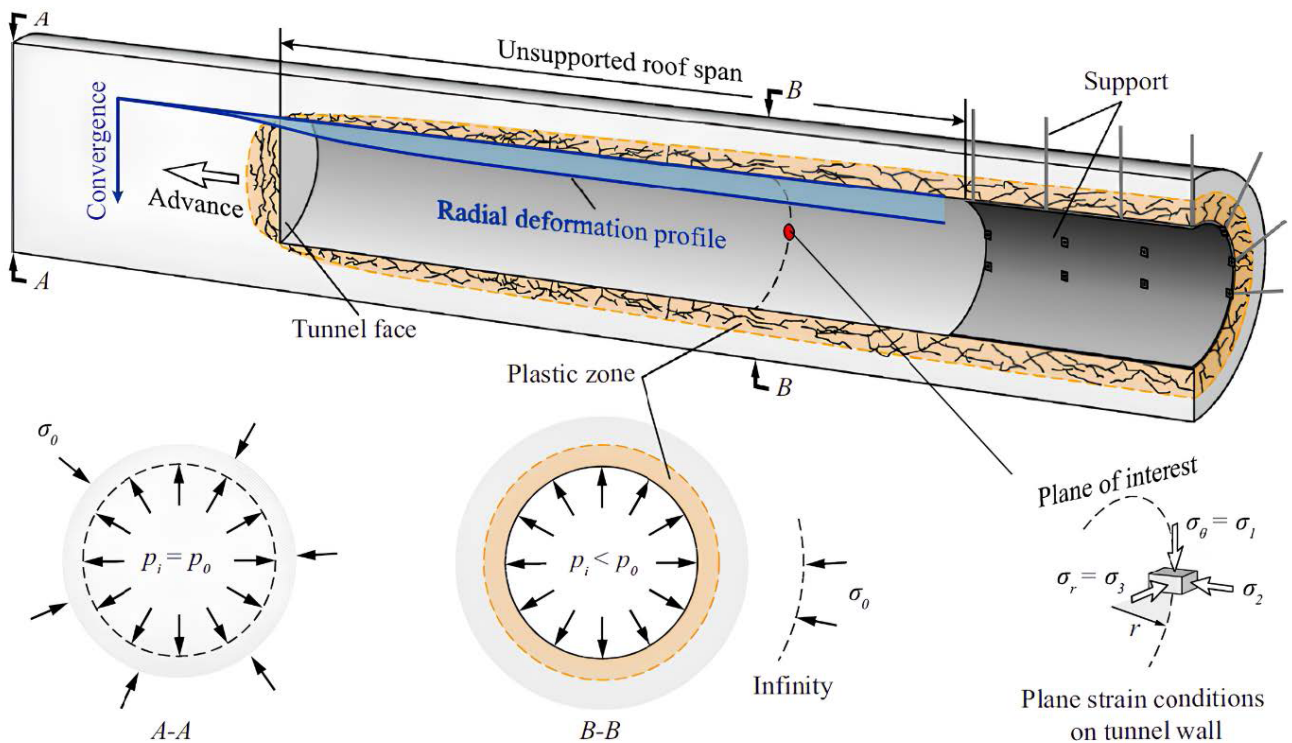


**Figure 2.** Stress profiles and radial displacement variations along the tunnel axis (Wang and Cai, 2022)

The relationship between this hypothetical pressure and the radial displacement at the tunnel wall is explained by the ground reaction curve (GRC), and the longitudinal displacement profile (LDP) is used to describe the relationship between

the change in radial displacement along the tunnel due to the advancement of the tunnel face (Figure 3). For any section along the tunnel, the pressure and displacement at the tunnel wall can be estimated if the LDP and GRC of the tunnel are known.

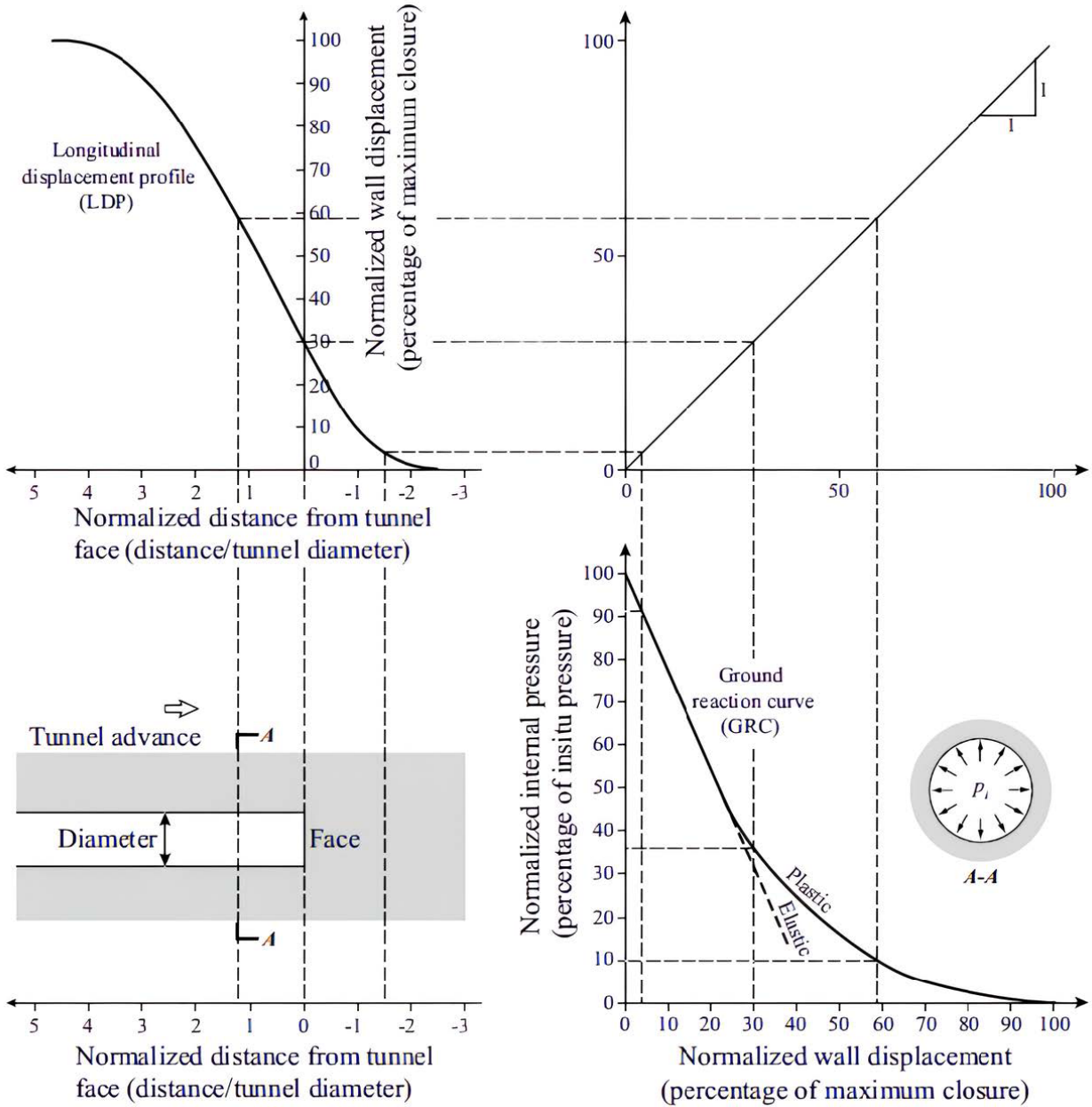


**Figure 3.** The convergence-confinement method (Wang and Cai, 2022)

### 1.3. Finite Element Modeling

Based on the data described in the previous subsection, tunnels in different rock masses were modeled in RS2 as summarized in Table 1. The analysis type is plane strain, the solver type is the “Gaussian Elimination Method”, and units are metric and MPa for stresses. For stress analysis, the maximum num-

ber of iterations was determined as 500 and the tolerance was 0.01. The “Generalized Hoek Brown” failure criterion was chosen while selecting the properties of the rock mass. Since the depth of the modeled tunnels is quite deep from the surface (the nearest tunnel is 130 m), movements are restricted on all sides. GRCs were obtained from RS2 for com-

parison with CCM. For this reason, using the stress reduction method, the pressures that will affect the support are added in 10 stages in a way that will decrease analytically. The mesh type is graded,

and the element type is a 3-node triangle. The finite element model of the tunnel is created in RS2 as shown in Figure 4.

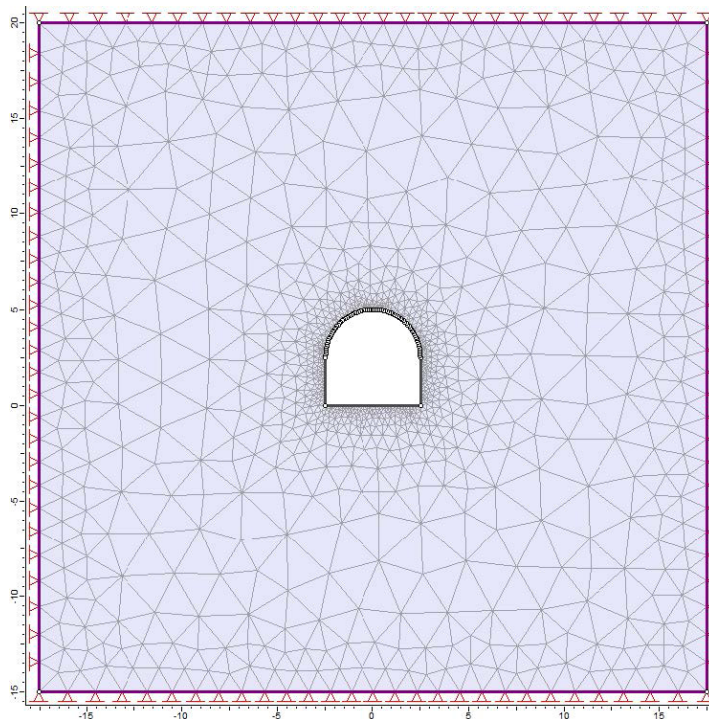


**Figure 4.** Finite element modeling

## 2. Results and Discussion

The radius of the plastic zone was determined according to the finite element model. According to the maximum displacement amount obtained from the model, the displacement amount correspon-

ding to the pressure that will affect the support was calculated by using the LDP curves drawn by the equations of Vlachopoulos and Diederichs (2009). These values obtained for three different rock masses are given in Table 2.

**Table 2.** LDP parameters of different rock masses used in the analyses

Parameters		Weak	Medium	Good
Plastic zone radius (m)	$R_p$	6.73	3.93	3.58
Tunnel radius (m)	$R_t$	2.5	2.5	2.5
$R_p/R_t$		2.7	1.6	1.4
Maximum displacement (m)	$U_{max}$	0.118	0.0038	0.0024
Displacement (m)	$U$	0.059	0.0024	0.0017
$U/U_{max}$		0.5	0.63	0.72

In order to make a comparison between CCM and FEM in terms of GRCs, GRCs were obtained by constructing the hypothetical  $p_i$  pressure in the FEM model. Since CCM is only recommended for fully circular underground openings, GRCs were

obtained by constructing circular-section FEM models with the same opening as horseshoe-section galleries. All GRCs generated for 3 different rock masses are given in Figures 5 to 7.

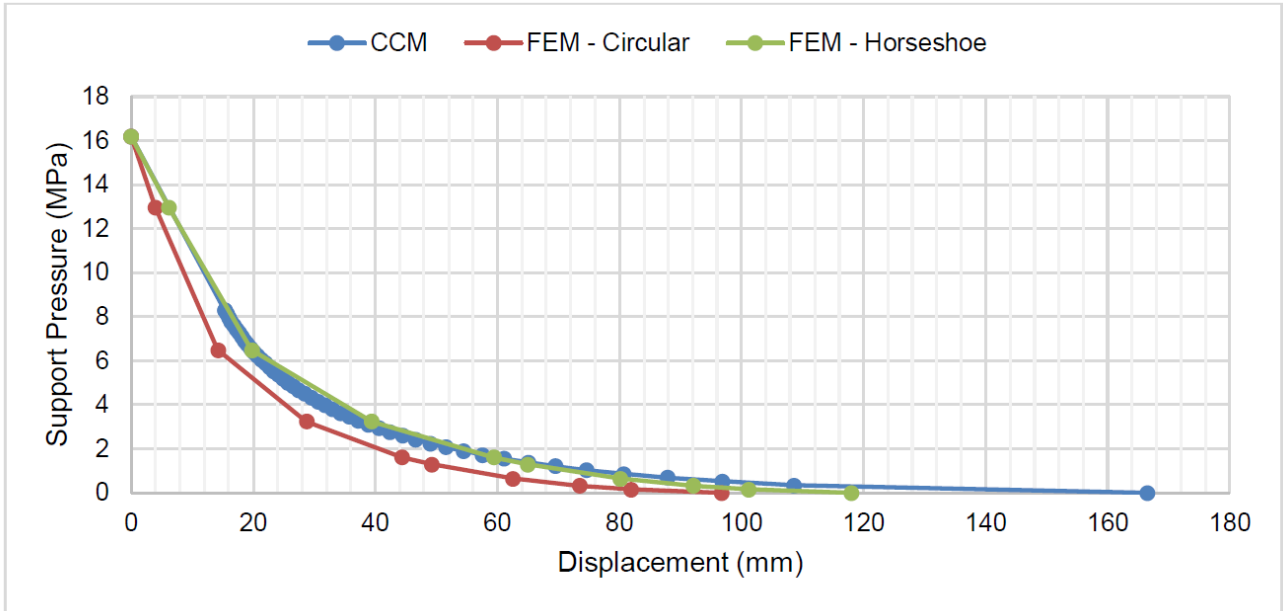


**Figure 5.** Ground reaction curves for weak rock mass

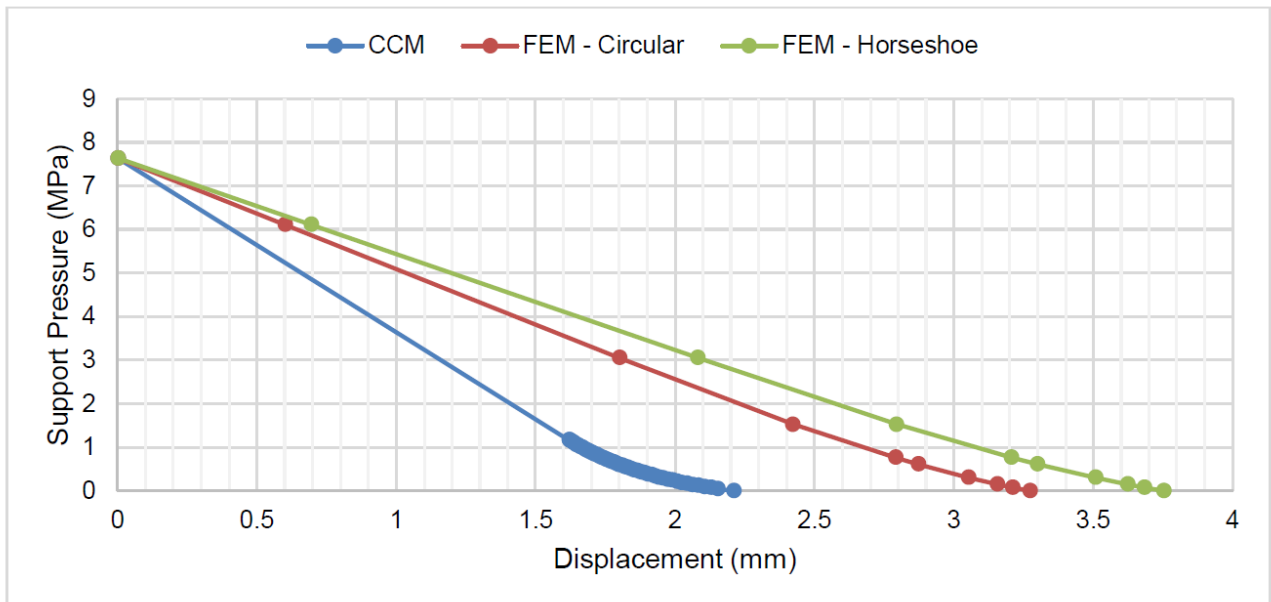


**Figure 6.** Ground reaction curves for medium rock mass

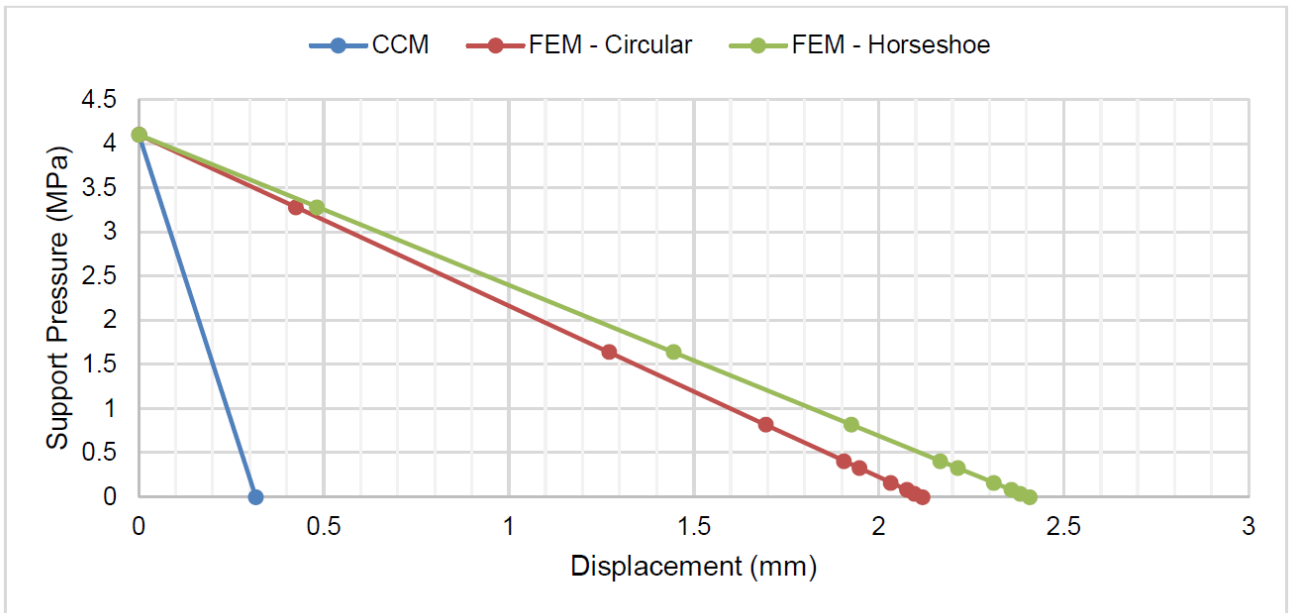


**Figure 7.** Ground reaction curves for good rock mass

Support pressures corresponding to the displacement amounts in Table 2 were calculated for all generated GRCs and the results are given in Table 3. The displacement amounts obtained from the FEM model for medium and good rock masses are greater than those calculated in the CCM and are therefore expressed as 0 in the table. It seemed that from Table 3, there is a correlation between the support pressures in the CCM and the horseshoe section FEM model. Based on this phenomenon, CCM and FEM support pressures corresponding to the same

displacements for the weak rock mass were compared. As a result of the comparison in Figure 8, it is seen that the support pressures obtained from CCM and FEM have a relationship with a high and reliable coefficient of determination. CCM and FEM displacements corresponding to the same support pressures were compared from the same point of view. A strong coefficient of determination has been found in the relationship among the displacements produced from CCM and FEM as an outcome of the comparison in Figure 9.

**Table 3.** Support pressures for different rock masses

Analyze	Support Pressure (MPa)		
	Weak	Medium	Good
CCM	1.60	0	0
FEM - Horseshoe	1.60	2.40	1.20
FEM - Circular	0.80	1.50	0.80

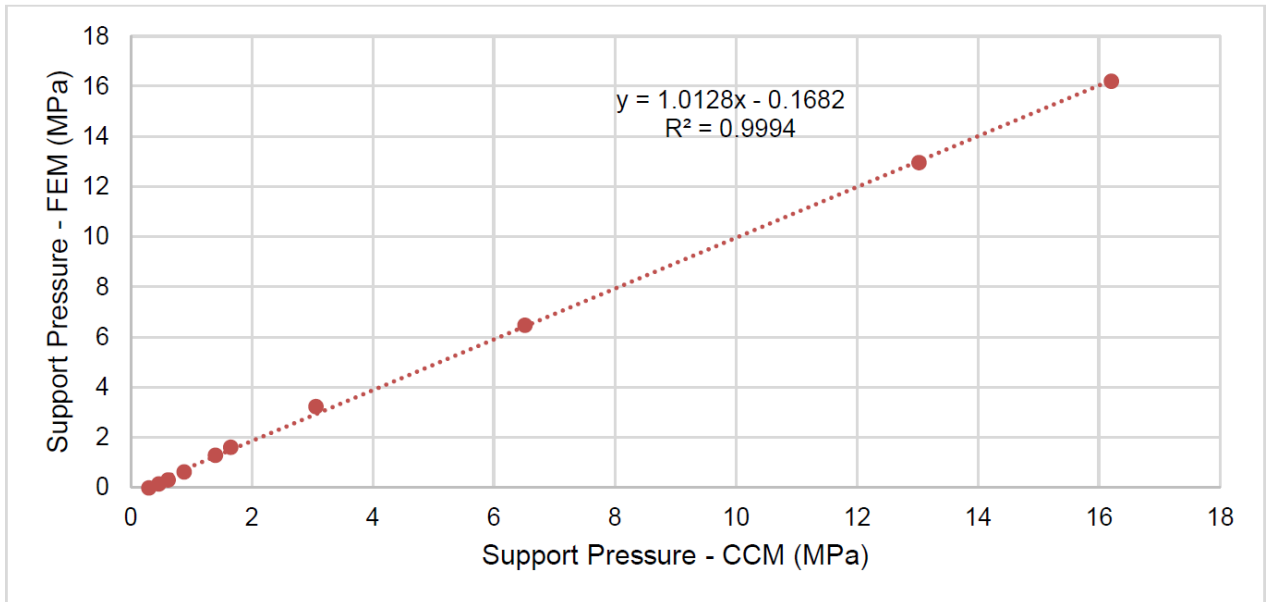


**Figure 8.** Relationship between CCM and FEM model in terms of support pressures for weak rock mass

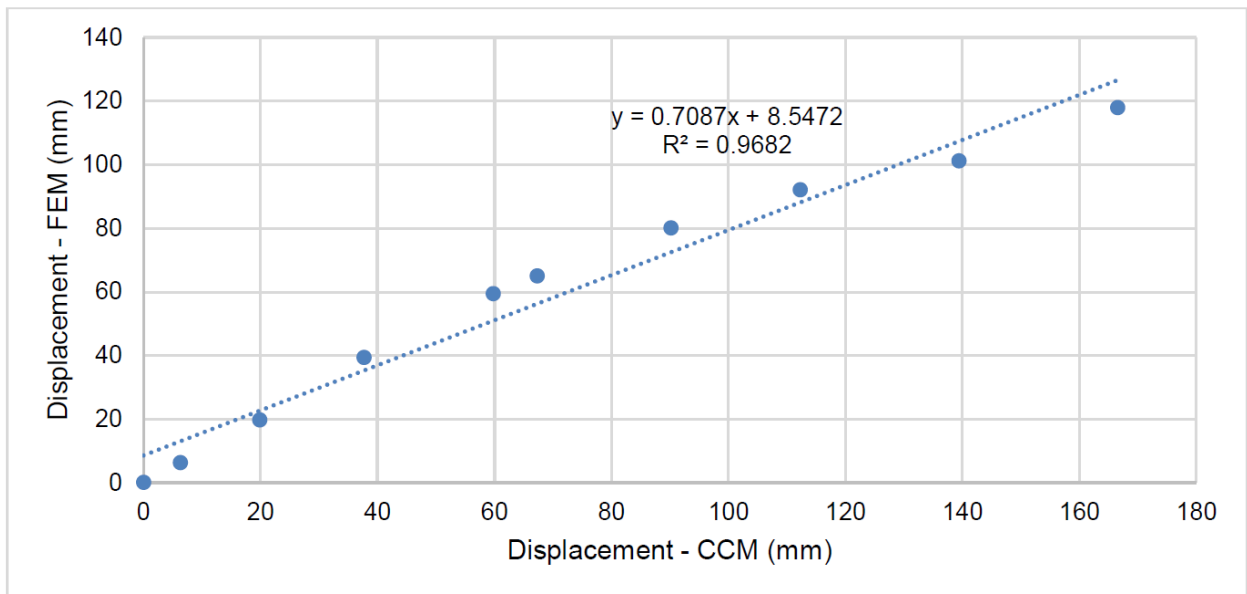


**Figure 9.** Relationship between CCM and FEM model in terms of displacements for weak rock mass

### 3. Conclusion

The finite element method and convergence-confinement method were used to estimate the support pressures in three different rock masses. The results obtained from the two methods are compared and the remarkable results are summarized below.

- It has been revealed that there is a high correlation in terms of support pressures and displacements between the horseshoe section FEM model created for the weak rock mass and the CCM.
- FEM models for medium and good rock masses

estimated more displacement than CCM. For this reason, it was not possible to make a comparison for good and medium rock masses.

- In order to make a better comparison with the CCM, circular cross-section FEM models were created with the same opening as the horseshoe cross-section models, but the horseshoe cross-section FEM model with the CCM gave more consistent results.
- It is seen that for rock masses with properties similar to the weak rock mass modeled in this study, the support pressures and displacements can be estimated with CCM, which is more practical than FEM.

## Acknowledgments

This study is a part of the first author's MSc. Thesis and was supported by Scientific Research Projects Coordination Unit of the Istanbul Technical University (ITU BAP) with a grant number in MYL-2021-43070. The authors thank to ITU BAP for financial support.

## References

- Aydan, Ö., Ulusay, R., & Tokashiki, N. (2014). A new rock mass quality rating system: rock mass quality rating (RMQR) and its application to the estimation of geomechanical characteristics of rock masses. *Rock mechanics and rock engineering*, 47, 1255-1276.
- Aygar, E. B. (2022). Zayıf zeminlerde açılan büyük çaplı çift tüp tünellerde tünellerin birbirine olan etkisinin 3 boyutlu sayısal analizler ile incelenmesine bir örnek, Bolu Tüneli destek sistemlerinin değerlendirilmesi. *Scientific Mining Journal*, 61(3), 157-168.
- Barton, N., Lien, R., & Lunde, J. J. R. M. (1974). Engineering classification of rock masses for the design of tunnel support. *Rock Mechanics*, 6, 189-236.
- Bieniawski, Z. T. (1973). Engineering classification of jointed rock masses. *Civil Engineering= Si-viele Ingenieurswese*, (12), 335-343.
- Birön, C., Arıoğlu E. (1985). *Madenlerde Tahkimat İşleri ve Tasarımı*, Birsen Kitabevi, İstanbul.
- Brown, E. T., Bray, J. W., Ladanyi, B., & Hoek, E. (1983). Ground response curves for rock tunnels. *Journal of Geotechnical Engineering*, 109(1), 15-39.
- Carranza-Torres, C., & Fairhurst, C. (2000). Application of the convergence-confinement method of tunnel design to rock masses that satisfy the Hoek-Brown failure criterion. *Tunnelling and underground space technology*, 15(2), 187-213.
- Cui, L., Yang, W., Zheng, J., & Sheng, Q. (2023). Improved equations of ground pressure for shallow large-diameter shield tunnel considering multiple impact factors. *Tunnelling and Underground Space Technology*, 138, 105166.
- Deere, D. U. (1964). Technical description of rock cores for engineering purpose. *Rock Mechanics and Engineering Geology*, 1(1), 17-22.
- Deere, D. U., Peck, R. B., Parker, H. W., Monsees, J. E., & Schmidt, B. (1970). Design of tunnel support systems. *Highway Research Record*, (339).
- Goel, R. K., Jethwa, J. L., & Dhar, B. B. (1996). Effect of tunnel size on support pressure. *International Journal of Rock Mechanics and Mining & Geomechanics Abstracts*, 33(7).
- Goel, R. K., Jethwa, J. L., & Paithankar, A. G. (1995). Indian experiences with Q and RMR systems. *Tunnelling and Underground Space Technology*, 10(1), 97-109.
- Hoek, E., & Brown, E. T. (1997). Practical estimates of rock mass strength. *International journal of rock mechanics and mining sciences*, 34(8), 1165-1186.
- Hoek, E. (2000). *Practical rock engineering* (2023 ed.). Rocscience, Toronto, available online at: <http://www.rocscience.com>.
- Huang, M., Li, Y., Shi, Z., & Lü, X. (2022). Face stability analysis of shallow shield tunneling in layered ground under seepage flow. *Tunnelling and Underground Space Technology*, 119, 104201.
- Jalote, P.M., Kumar A., Kumar V. (1996). Geotechniques applied in the design of the machine hall cavern, Nathpa Jhakri Hydel Project, N.W. Himalaya, India. *J. Engng Geol. (India)* XXV(1-4), 181-192.
- Kumar, B., & Sahoo, J. P. (2023). Lining pressure for circular tunnels in two layered clay with anisotropic undrained shear strength. *Geomechanics and Geoengineering*, 18(2), 91-104.
- Lauffer, H. (1958). Gebirgsklassifizierung für den stollenbau. *Geologie und Bauwesen*, 24(1), 46-51.
- Moretto O., Sarra Pistone R.E. and Del Rio J.C. 1993. A case history in Argentina - Rock mechanics for underground works in the pumping storage development of Rio Grande No 1. In *Comprehensive Rock Engineering*. (Ed. Hudson, J.A.) 5, 159- 192. Oxford: Pergamon.

- Niu, Y., Ren, T., Zhou, Q., Jiao, X., Shi, J., Xiang, K., ... & Satyanaga, A. (2023). Analysis of Excavation Parameters on Face Stability in Small Curvature Shield Tunnels. *Sustainability*, 15(8), 6797.
- Palmstrom, A. (1995). Characterizing the strength of rock masses for use in design of underground structures. In *International conference in design and construction of underground structures* (Vol. 10).
- Palmstrom, A. (2000). Recent developments in rock support estimates by the RMI. *Journal of Rock Mechanics and Tunnelling Technology*, 6(1), 1-19.
- Panet, M., & Guellec, P. (1974). Contribution to the problem of the design of tunnel support behind the face. *Progres en mecanique des roches-comptes rendus du 3eme congres de la societe internationale de mecanique des roches*, Denver.
- Panet, M., & Sulem, J. (2022). *Convergence-confinement method for tunnel design*, Switzerland: Springer.
- Panet, M., Givet, P. D. C. O., Guilloux, A., Duc, J. L. D. G. N. M., Piraud, J., & Wong, H. T. S. D. H. (2001). The convergence-confinement method. *AF-TES-recommendations des Groupes de Travail*.
- Protodyakonov, M. M. (1907). *Rock pressure on mine support (theory of mine support)*. Tipografiya Gubernskogo Zemstva, Yekaterinoslav, 23-45.
- Rocscience. (2020a). *RS2, Version 11*. Toronto, Ontario, Canada.
- Rocscience. (2020b). *RocSupport, Version 5*. Toronto, Ontario, Canada.
- Rose, D. (1982). Revising Terzaghi's tunnel rock load coefficients. In *The 23rd US Symposium on Rock Mechanics (USRMS)*. OnePetro.
- Seshagiri Rao, K. (2020). Characterization, modeling and engineering of rocks and rockmasses. *Indian Geotechnical Journal*, 50, 1-95.
- Sharma, S., Muthreja, I. L., & Yerpude, R. R. (2020). Application and comparison of squeezing estimation methods for Himalayan tunnels. *Bulletin of Engineering Geology and the Environment*, 79, 205-223.
- Singh, B., Goel, R. K., Jethwa, J. L., & Dube, A. K. (1997). Support pressure assessment in arched underground openings through poor rock masses. *Engineering Geology*, 48(1-2), 59-81.
- Stille, H., Groth, T., & Fredriksson, A. (1982). FEM-analysis of rock mechanical problems with JOBFEM. *Stiftelsen Bergteknisk Forskning-BeFo, Stockholm*, 307(1), 82.
- Taghizadeh, H., Zare, S., & Mazraehli, M. (2020). Analysis of rock load for tunnel lining design. *Geotechnical and Geological Engineering*, 38(3), 2989-3005.
- Terzaghi, K., Proctor, R. V., & White, T. L. (1946). *Rock tunneling with steel supports*. Commercial Shearing and Stamping Co, 119-140.
- Ünal, E., & Özkan, I. (1990). Determination of classification parameters for clay-bearing and stratified rock mass. In *Proceedings of the 9th International Conference on Ground Control in Mining*. Morgantown: West Virginia University (pp. 250-259).
- Vlachopoulos, N., & Diederichs, M. S. (2009). Improved longitudinal displacement profiles for convergence confinement analysis of deep tunnels. *Rock mechanics and rock engineering*, 42, 131-146.
- Wang, M., & Cai, M. (2022). Numerical modeling of stand-up time of tunnels considering time-dependent deformation of jointed rock masses. *Rock Mechanics and Rock Engineering*, 55(7), 4305-4328.
- Wickham, G. E., Tiedemann, H. R., & Skinner, E. H. (1972). Support determinations based on geologic predictions. In *N Am Rapid Excav & Tunnelling Conf Proc* (Vol. 1).
- Zhang, H., Zhang, G., Pan, Y., Hao, Z., Chen, S., & Cheng, F. (2022). Experimental study on the mechanical behavior and deformation characteristics of lining structure of super-large section tunnels with a small clearance. *Engineering Failure Analysis*, 136, 106186.



## Enhancing the bearing capacity of friction anchor bolts through cementitious concrete injection for reinforced support in Imiter underground rock masses

Amine Soufi<sup>a,\*</sup>, Youssef Zerradi<sup>a,\*\*</sup>, Mohammed Souissi<sup>a,\*\*\*</sup>, Latifa Ouadif<sup>a,\*\*\*\*</sup>, Anas Bahi<sup>a,\*\*\*\*\*</sup>

<sup>a</sup>Mohammed V University, Rabat, MOROCCO

Received: 10 June 2023 \* Accepted: 9 October 2023

### ABSTRACT

Friction anchor bolts are commonly used to provide support in underground structures by relying on frictional forces between the bolt and the surrounding rock. This study proposes a method to enhance the efficiency of these bolts by injecting a cement-based mixture comprising cement, sand, and additives. The injection of this mixture into the bolt results in internal expansion, which reinforces the friction and bearing capacity of the bolt. The increased volume exerts a radial force, leading to improved adherence, load transfer, and void filling. Pullout tests were conducted on various rock masses to evaluate the performance of the anchor bolts. The results demonstrate increased pullout resistance with higher rock mass quality and longer cemented bolts. Additionally, the use of a silicate-based additive accelerated the curing time of the cement, enhancing the strength of the bolts. The study also highlights the significant influence of groundwater on the bearing capacity of the bolts. These findings indicate the effectiveness of cemented concrete injection in strengthening friction anchor bolts and their anchorage in underground structures.

**Keywords:** Friction anchor bolt, Cemented concrete injection, Additives, Pullout resistance

### Introduction

Friction anchor bolts play a critical role in providing support and stability to underground structures by utilizing the frictional forces between the bolt and the surrounding rock. However, there is a need to enhance the performance of these bolts to improve their bearing capacity (BC) and overall effectiveness. This study introduces a novel approach to enhance the efficiency of friction anchor bolts through the injection of a cement-based mixture (Li et al., 2016).

The proposed method involves injecting a cement-based mixture comprising cement, sand, and additives into the hollow profile of the friction anchor bolt. This injection leads to internal expansion, resulting in increased volume and reinforcing the frictional interaction between the bolt and the rock. The radial force exerted by the

expanded concrete improves the bolt's adherence, load transfer, and void filling capacity, thereby strengthening the anchor bolt and improving the stability of the support system (Liu et al., 2021).

Pullout tests were conducted on various rock masses to evaluate the performance of the cemented friction anchor bolts. These tests considered different rock mass qualities and bolt lengths to examine their impact on pullout resistance. The results revealed a positive correlation between rock mass quality and pullout resistance, indicating that higher-quality rock masses exhibit improved bearing capacity.

In addition, the curing time of the injected cement plays a crucial role in the effectiveness of the cemented friction anchor bolts. To address this, a silicate-based additive was incorporated into the cement mixture, accelerating the curing process.

\* Corresponding author: soufi@emi.ac.ma • <https://orcid.org/0009-0002-6137-9459>

\*\* zerradi@emi.ac.ma • <https://orcid.org/0000-0003-0192-8225>

\*\*\* rmsouissi@emi.ac.ma • <https://orcid.org/0000-0002-9117-7885>

\*\*\*\* ouadif@emi.ac.ma • <https://orcid.org/0000-0002-4613-1124>

\*\*\*\*\* a.bahi@emi.ac.ma • <https://orcid.org/0000-0002-1450-7254>

<https://doi.org/10.30797/madencilik.1312485>

This additive shortened the curing time, thereby enhancing the strength of the bolts and enabling immediate support.

Furthermore, the study investigated the influence of groundwater on the bearing capacity of the cemented bolts. It was found that groundwater significantly affects the performance of the bolts, emphasizing the importance of considering groundwater conditions in the design and application of cemented friction anchor bolts.

In conclusion, the proposed cemented concrete injection technique offers a promising approach to enhance the strength and anchorage of friction anchor bolts in underground structures. The findings of this study demonstrate the effectiveness of the cemented bolts in improving pullout resistance, bearing capacity, adherence, load transfer, and overall stability.

The incorporation of a silicate-based additive accelerates the curing time, further enhancing the strength of the bolts. Consideration of groundwater conditions is crucial for ensuring optimal performance. These results contribute to the understanding and advancement of friction anchor bolt technologies, offering potential benefits for the design and construction of underground structures.

## 1. Methods

### 1.1. Mine location

The Imiter silver mine is an underground mine situated in the Anti-Atlas Mountain range of Morocco, approximately 120 km southeast of the City of Ouarzazate. Located at an elevation of 1600 meters above sea level in a remote desert region, Imiter is the largest silver producing mine in Africa.

The extensive underground workings at Imiter reach depths exceeding 600 meters below surface across 11 production levels. The principal extraction methods employed are cut-and-fill and longhole open stoping. Significant geotechnical challenges encountered in the mine include high in-situ stresses and generally poor rock mass quality requiring extensive ground support.

The study site discussed in this paper is situated at the 500 meter level of the Imiter mine. The rock types encountered are dominantly volcanosedimentary in origin. Prominent foliation planes strike nearly uniformly east-west across the rock mass. Multiple discontinuity sets are present, with frequent intersection of the various fracture orientations.

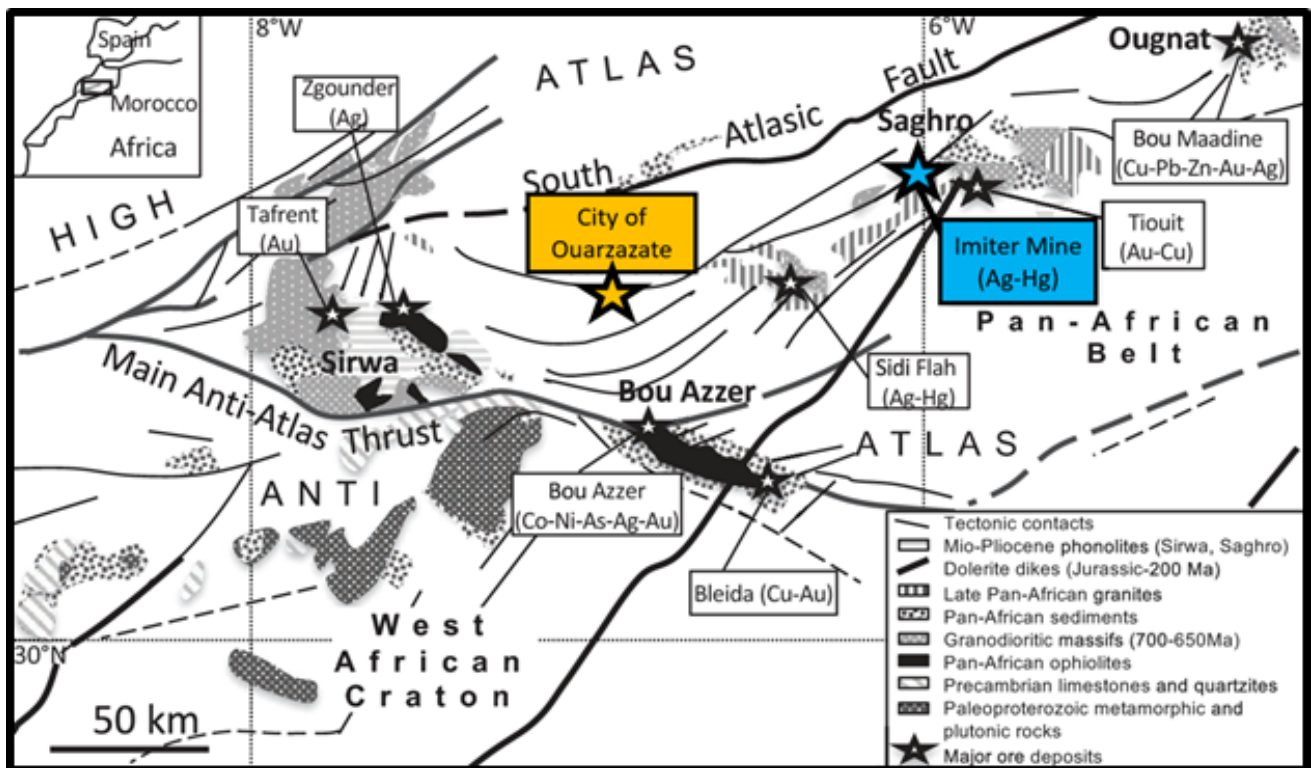


**Fig.1.** Geological Sketch map of the location of the major deposit and the mine location

### 1.2. Tested friction anchorage bolt

Friction bolts are hollow and thin metal profiles brought into intimate contact with the rock along their entire length, allowing for friction-based anchoring, their effectiveness is immediate. The Split Set (Figure 2.a) is a friction anchorage bolt for rocks

that is inserted within seconds by simple percussion into a hole slightly smaller in diameter than the tube. The straightness of the hole is not important. The bolt conforms to the irregularities of the terrain, provides significant friction through radial pressure along its entire length (Figure 2.b), and ensures immediate anchoring (Li et al., 2017).

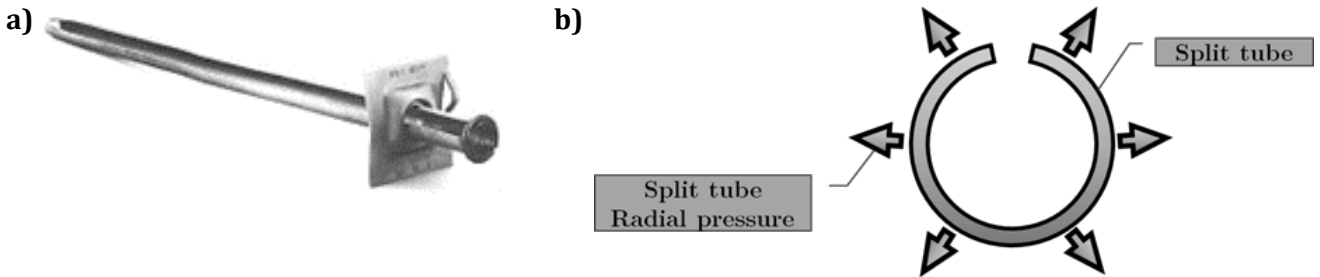


**Fig.2.** a) Friction bolt / Split set (Hoek, 1993) b) Radial pressure of the friction bolt

### 1.3. Principle of the test

The anchorage force of the anchorage bolt is generally evaluated using an extraction test, and the anchorage behavior of the anchorage bolt has been studied based on the load-displacement curves from the extraction test. An extraction load

is applied to the outer end of the anchorage bolt, and the displacement of the anchorage bolt is then measured.

The traction jack (Figure 3) consists of two main units: a mechanical part (grip, bell, threaded bar, spacer, and nut) and a hydraulic part (jack, pump, pressure gauge).

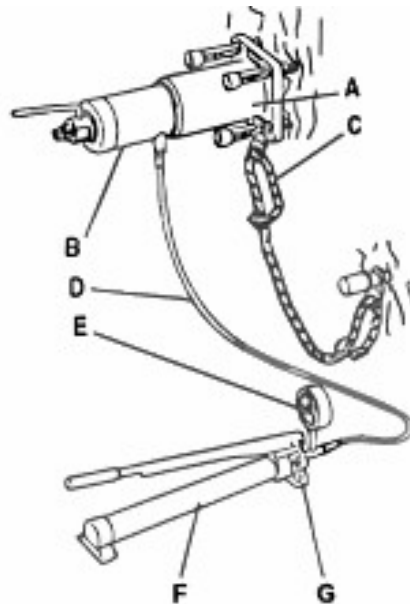


**Fig.3.** Pull-out test setup (A: Charging case - B: Jack - C: Safety chain - D: Hydraulic hose - E: Manometer - F: Hand pump - G: Valve)

The hole for an anchorage bolt is typically drilled perpendicular to the tunnel excavation surface. The drilling hole for the split set was drilled with a length of 1.8m, and a friction bolt was installed. The

grout used was a mixture of ordinary Portland cement and sand in a 1:1 ratio. Sand with a maximum particle size of 2 mm was used.

## 2. Theory

### 2.1 Enhancing Friction Bolt Adherence

By combining the pressure generated through the diameter difference between the holes and the bolt, our proposal aims to enhance the bolt's adherence to the rock mass by introducing a cementitious mixture consisting of cement, sand, and two

additives. This mixture will be injected into the friction bolt to ensure internal expansion, with the objective of improving friction and consequently the load-bearing capacity of the bolt. When the pressures generated by the expansion of the cemented mixture and the diameter gap between the bolt and the hole are combined (Figure 4).

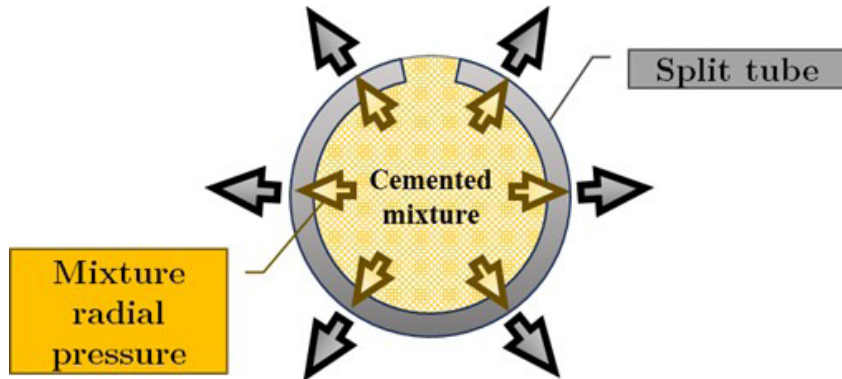


*Fig.4. Radial pressure of cementation mixture.*

Our tensile strength is naturally enhanced by confinement. When a friction anchor bolt is inserted into a hole in a rock mass, the rock exerts a radial confinement force on the bolt when it is tensioned. This force results from the elastic deformation of the surrounding rock (Figure 5). The radial confine-

ment increases the pressure exerted on the bolt, thus improving the friction between the bolt and the rock. This increased friction enhances the bolt's resistance to pull-out. Consequently, the anchorage is more stable and can better withstand external loads.

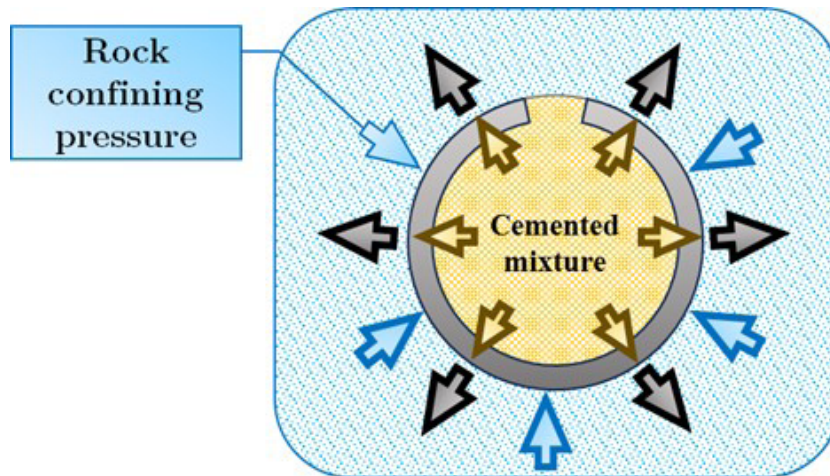


*Fig.5. Radial confining pressure of rock mass*

### 2.2 Cementitious Mixture Injection

In the present study, we propose the injection of friction bolts with concrete and two types of additives for two objectives. Firstly, to accelerate the consolidation of concrete in a very short time, and secondly, and most importantly, to enhance the increase in volume of concrete as a function of consolidation over time. These additives are designed to induce controlled expansion of the concrete, leading to a specific volume increase.

**Silicate-based additives:** Alkali silicates can also be used to accelerate concrete consolidation. These additives react with cement components to form reaction products that promote faster setting.

**Gypsum-based expansive additives:** These additives contain gypsum (calcium sulfate dihydrate), which reacts with water present in the concrete to form expansive crystals. These crystals create internal pressure that increases the volume of the concrete. Gypsum-based additives are often used to

compensate for subsequent plastic shrinkage of the concrete.

When our concrete is injected inside a bolt anchored in rock, its volume increases over time due to chemical hydration reaction and the gypsum-based additive.

This increase in concrete volume exerts a radial force inside the bolt, directed towards the rock mass. This radial force has several beneficial effects on the bolt's pull-out resistance:

**Increased adhesion:** The radial force exerted by the increased volume of concrete promotes better adhesion between the bolt and the rock mass. This improved adhesion strengthens the bolt's ability to resist pull-out forces.

**Load transfer:** The radial force transmitted by the concrete expansion helps transfer applied loads on the bolt to the rock mass. This reduces local stresses on the bolt and contributes to a better distribution of forces, enhancing overall pull-out resistance.

**Void filling:** During concrete injection, voids may exist inside the bolt and between the bolt and the rock. Concrete expansion helps fill these voids and ensure closer contact between the bolt and the rock, thus improving anchorage efficiency.

**Increased stability:** The increase in concrete volume can also contribute to greater overall stability of the support system. By reinforcing the bolt anchorage, the concrete reduces undesired movements or deformations of the bolt and rock mass, thereby improving the strength and durability of the support structure.

In summary, the volume increase of concrete injected into an anchored bolt promotes adhesion to the rock mass, transfers loads, fills voids, and enhances the overall stability of the support system. These combined effects contribute to strengthening the bolt's pull-out resistance and ensuring effective anchorage in the rock.

### 3. Results and discussion

#### 3.1 Behavior of bolts in a dry rock mass

The Rock Mass Rating (RMR) system was developed by Bieniawski in the 1970s to provide a quantitative estimate of rock mass quality based on six parameters: uniaxial compressive strength of intact rock, RQD (rock quality designation), spacing of discontinuities, condition of discontinuities, groundwater conditions, and orientation of discontinuities.

The six parameters are rated and summed to give an overall RMR value between 0-100 which is correlated with rock mass classes and estimated engineering properties. A higher RMR indicates better, more competent rock mass conditions (Bieniawski, 1988).

The Q-System was developed by Barton, Lien, and Lunde in the 1970s to complement the RMR system. It aims to quantify the quality of the rock mass to provide estimates of support requirements. It involves rating six parameters on a logarithmic scale: RQD, joint set number (Jn), joint roughness number (Jr), joint alteration number (Ja), joint water reduction factor (Jw), and stress reduction factor (SRF). The sum of the six parameters gives the Q-value, which ranges from 0.001 to 1000. A higher Q indicates better quality rock mass with lower support requirements (Barton et al., 1981).

To investigate the anchoring and traction behavior of an anchorage bolt in a dry rock (Figure 6), several field tests were conducted at the Imiter mining site in Morocco. This section includes nine pull-out tests on three anchors in each rock mass RMR=40, RMR=60, and RMR=80. The primary rock component is sandy siltstone, and the joint spacing is classified as dense, with soft filling materials.



*Fig.6. Pullout test*

The behavior of anchorage bolts was studied by analyzing the load-displacement relationship in the extraction test. The effect of each dry rock mass on the behavior of the anchorage cemented bolt was examined by comparing the extraction resistance and displacement at the yield limit. The Figure 7 depict the relationship between extraction load and displacement for each rock condition. The extraction resistance was determined following ASTM standard D443513e1.

RMR=40 ; Q=0,5

RMR=60 ; Q=5

RMR=80 ; Q=10

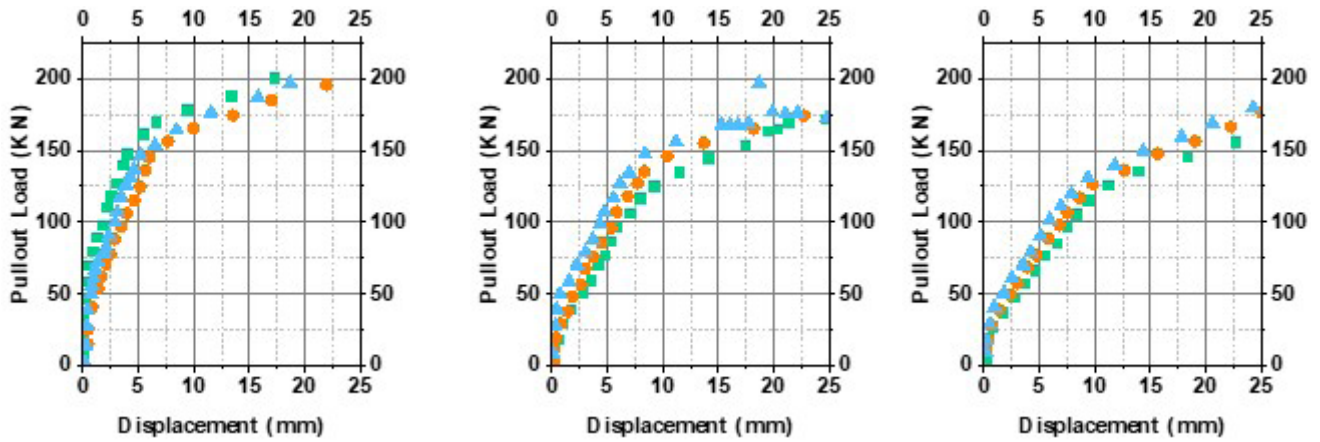


**Figure 7.** a) Pullout load-displacement for RMR=40; b) Pullout load-displacement for RMR=60; c) Pullout load-displacement for RMR=80

The test results demonstrate that the slope of the load-displacement curve increases with the improvement of rock mass quality, leading to an increase in pull-out resistance. This trend was more pronounced when the tested dry rock mass became more competent (stiffer).

The detection of the pullout failure point of cemented friction bolts was achieved by observing the change in slope of the load-displacement curve (Figure 8). The upper (abc) and lower (a'b'c') boundaries were plotted, correlating the two inflection points (bb'), in order to obtain the failure line:

$$BC \text{ (KN)} = 1,32RMR + 60 \tag{1}$$

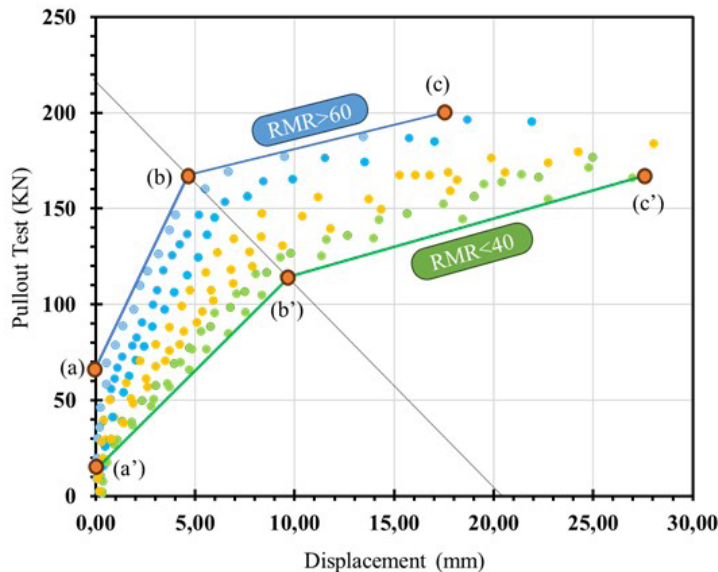


**Fig.8.** Pullout load-displacement for RMR=40, RMR=60 and RMR=80

### 3.2 Effect of bolt length and Rock Mass Quality

The pullout capacity of friction rock bolts increases with length, but at a diminishing rate. Longer bolts exhibit higher load capacity but lower strength per unit length. The paper provides

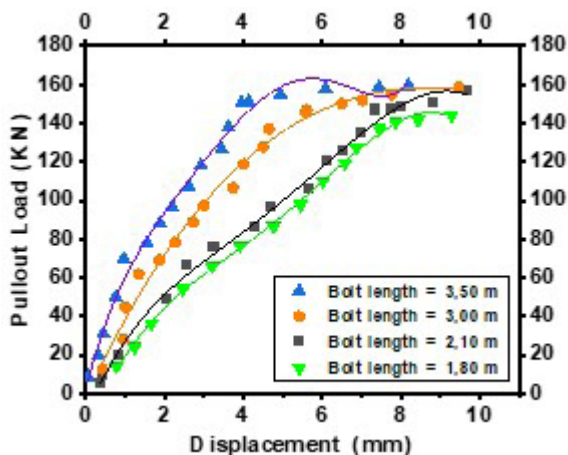
equations relating bolt length to pullout resistance based on numerical modeling and field pull-out tests (Komurlu and Demir, 2019).

The relationship between anchorage bolt length and load-displacement response was in-

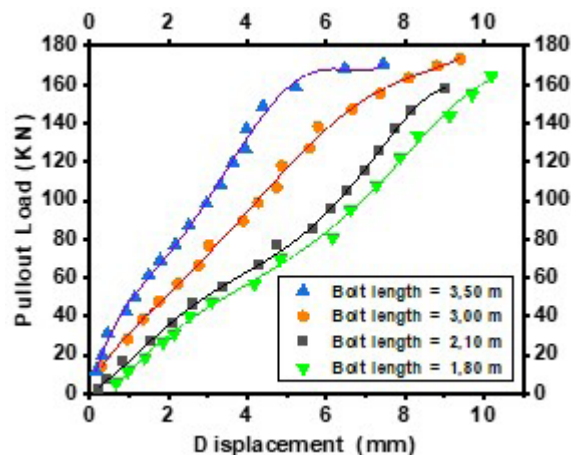
investigated in rock masses of varying quality, categorized using Bieniawski's Rock Mass Rating (RMR) system and Barton's Q-system. The influence of cemented anchorage bolt length on traction behavior was investigated in moderate and

soft rocks with lengths ranging from 1.8 to 3.5 m. Figure 9 depicts the relationship between pull-out load and displacement for various anchorage bolt lengths.

a) RMR=40 ; Q=0,5



b) RMR=60 ; Q=5



c) RMR=80 ; Q=10

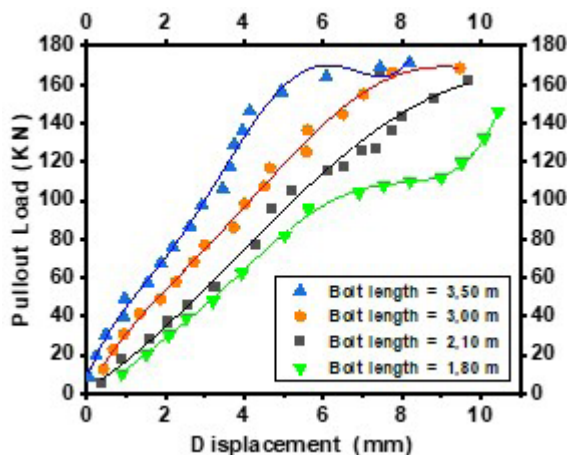


**Fig. 9.** Pullout load-displacement with lengths ranging for a) RMR=40 b) RMR=60 and c) RMR=80

The slope of the load-displacement curve increased with bolt length in rock masses with RMR values of 40 (Q=0.5), 60 (Q=5), and 80 (Q=10). This illustrates an increase in yield limit load capacity linked with longer bolt installations across poor, fair, and good quality rock masses. The study emphasizes the advantages of longer anchor lengths, especially in short bolts, for increasing load capacity (Figure 9).

To prevent having a negative residual value ( $b < 0$ ) in the regression equations ( $y = a \cdot B^b$ ) for different

rock mass qualities, a constraint was imposed requiring zero bearing capacity at negligible bolt lengths. This origin-passing condition forces all regression lines through the point (0,0) on the plot of bolt length versus capacity. Anchoring the regressions at zero eliminates the possibility of a negative y-intercept term (b), which is non-physical given that bolts cannot provide negative support. Extrapolating the regressions to zero length must correspond to zero capacity for consistency with expected mechanical

behavior. Constraining the regressions to intersect (0,0) also enhances fit and predictive performance by eliminating unrealistic negative residuals (Figure 10).

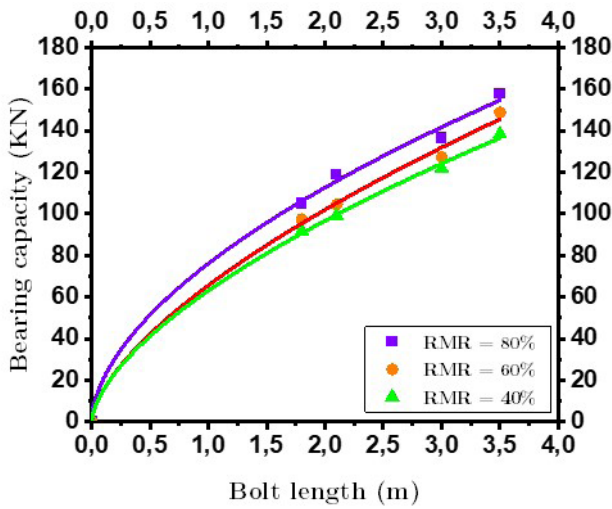


**Fig. 10.** Pull-out bearing capacity with lengths ranging

Overall, requiring the regression lines to pass through the origin provides a sensible bounding condition that improves representation of the relationship between bolt length and bearing capacity across different rock masses. To estimate the carrying capacity of cemented friction bolts, taking into account the cemented bolt length and the quality of the rock mass, the following expression is proposed:

$$BC_{Bl} \text{ (KN)} = a \cdot Bl^b \quad (2)$$

Where:

BC: bearing capacity (KN)

Bl: cemented bolt length (m)

**Table 1.** Parameter of adjusted exponential model

Parameters	Optimized Values		
	RMR=80	RMR=60	RMR=40
<b>a</b>	76,12 ± 5,59	65,63 ± 4,7	63,04 ± 2,6
<b>b</b>	0,56 ± 0,07	0,63 ± 0,07	0,61 ± 0,04
<b>r<sup>2</sup></b>	0,95	0,96	0,98

To account for the combined effect of both fully grouted bolt length and rock mass quality (RMR) on bearing capacity, a 3D surface plot was generated interpolating between available measurement points. This allowed visualization of bearing capacity as a function of the two parameters of interest. The 3D representation captures how bolt length and RMR

quality interact to influence capacity, generating the interpolated surface enabled continuous prediction of bearing capacity across varied bolt lengths and rock mass ratings based on the measured data.

The 3D interpolation and surface plotting methodology enable straightforward interpretation of capacity trends in response to concurrent changes in bolt geometry and rock mass characteristics. Fitting the following proposed model allows representing the combined effect of length and RMR on capacity in a closed-form equation.

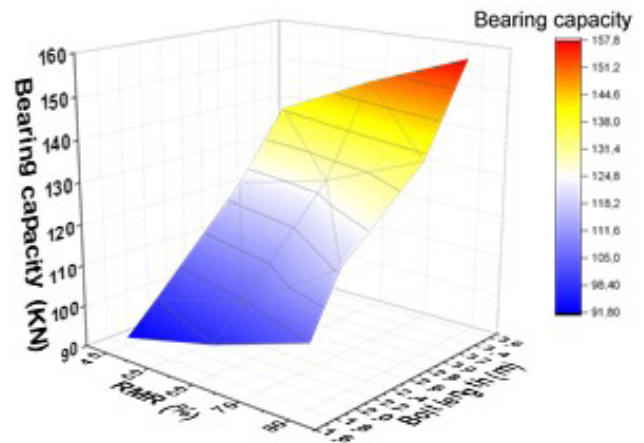
$$BC_{(RMR,Bl)} \text{ (KN)} = A + \frac{B}{\left[1 + e^{\left(\frac{C-RMR}{D}\right)}\right] \left[1 + e^{\left(\frac{E-Bl}{F}\right)}\right]} \quad (3)$$

Where:

BC: bearing capacity (KN)

Bl: cemented bolt length (m)

a)



b)

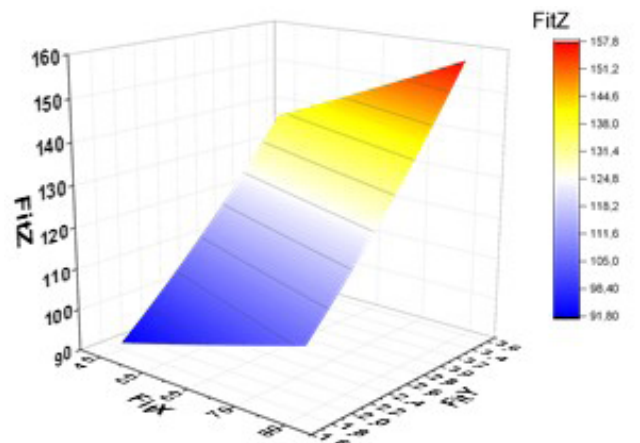


**Fig. 11.** a) 3D surface interpolation from pullout measurement points, b) 3D surface plotting of fitted exponential model

Multiple regressions were performed to identify the coefficients values that maximized the Pearson correlation coefficient ( $r^2=0,96$ ), thereby ensuring acceptable prediction accuracy compared to measurements.

**Table 2.** Parameter of adjusted regression model

Parameters	Optimized Values
A	$-1,88 \pm 106,8$
B	$3827,16 \pm 59261,9$
C	$236,61 \pm 4209,6$
D	$236,61 \pm 4209,6$
E	$10,7 \pm 49,3$

The proposed exponential formulation with optimized coefficients provides a predictive relationship able to capture the interactive effects between bolt length and rock mass quality based on the empirically measured capacities. This exponential model enables straightforward estimation of bearing capacity across the range of tested bolt lengths and rock mass ratings.

### 3.3 Effect of Curing Time on Cemented Anchor Bolts

The setting time of injected cement is an important issue in the application of cemented anchor bolts. It affects the stabilizing capacity of the bolts. Cement takes time to set and harden; therefore, cemented bolts cannot be used for immediate support.

Kilic et al. conducted traction tests on eight groups of bolts with the same length and mortar with a water-to-cement ratio of 0.4. They were tested to determine the effects of curing time on bolt bond strength. Each group of bolts had a different curing time. The results showed that during the first 7 days, the bond strength of the bolts and the maximum traction load increased rapidly. After 7 days, the tests continued to increase but at a slower rate (Kilic et al., 2002).

To address the issue related to setting time, a decision was made to add a silicate-based admixture to accelerate the consolidation process. Subsequently, a series of pull-out tests was conducted on six cemented bolts, distributed in two different types of rock masses characterized by quality indices RMR=40 and RMR=60. The displacements of the installed bolts were then recorded at three distinct time intervals: after 24 hours, 48 hours, and 72 hours (Figure 12).

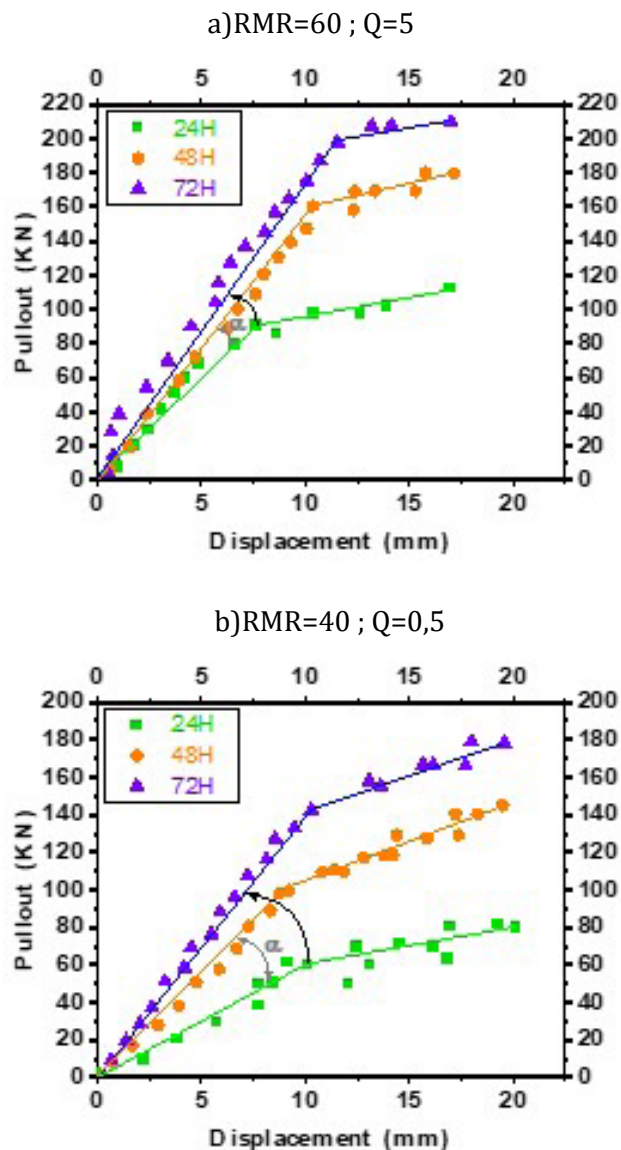


**Fig. 12.** Pull-out bearing capacity with lengths ranging a) RMR=60 b) RMR=40

For an RMR=40 rock mass, it is evident that the bearing capacity experienced a significant increase, rising from 80 kN to 160 kN after a period of 72 hours following the installation of the cemented bolt.

The results obtained clearly demonstrated a significant increase in bearing capacity after the installation of the cemented bolt over a 72-hour period. Initially, the bearing capacity was 100 kN, but it increased significantly to reach 200 kN. In other words, we observed a 100% improvement in bearing capacity between the first and third day.

The first observation regarding Figure 11 is that within the same RMR class, the slope of the pull-out-displacement curve increases as a function of curing time. Furthermore, quantitative analysis

reveals a decrement in the angular divergence  $\alpha$  between directing slopes of pullout-displacement curves as RMR score improves. In other words, the pullout-displacement lines converge angularly over time when moving from lower to higher RMR values. This suggests a closing of the angular separation between pullout-displacement relationships as curing duration increases, particularly for rock masses of greater quality per the RMR classification.

The diagram depicted Figure 13 illustrates the correlation existing between the bearing capacity and curing time for two distinct classes of Rock Mass Rating (RMR), to estimate the bearing capacity of cemented friction bolts, taking into account the curing time and the quality of the rock mass, the following expression is proposed:

$$BC(KN)=1,7Ct+1,3 RMR - 25 \quad (4)$$

Where:

BC: bearing capacity (KN)

Ct: curing time (hours)

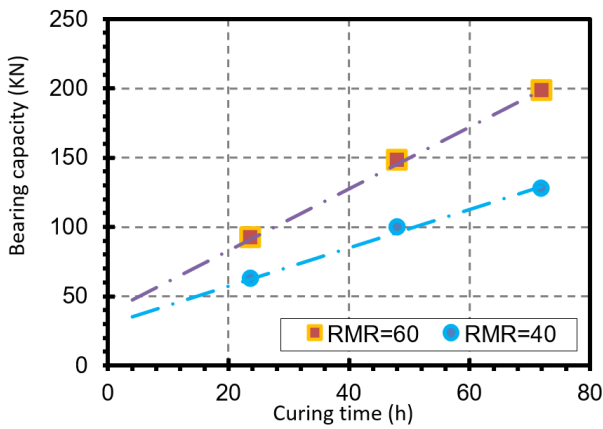


**Fig.13.** Pull-out bearing capacity with Curing Time

These results indicate that the setting time plays a crucial role in enhancing the strength of the cemented bolt. The analysis of the obtained data significantly confirms the positive effect of setting time on the strength of the cemented bolt.

### 3.4 Impact of groundwater on bearing capacity

Zhang et al. studied the impact of groundwater on the load-bearing capacity of anchor bolts in a coal mine, using the rating of water condition (Rw) index of the RMR classification to estimate the water flow in the underground structures of the mine. The results showed that the presence of groundwater had a significant impact on the load-bearing capacity of the anchor bolts (Zhang et al., 2017).

The Rw rating of water condition is a parameter used in the Rock Mass Rating (RMR) system for rock mass classification. It was introduced by Z.T. Bieniawski in 1973 and provides a quantitative estimate of the quality of water seeping through rock discontinuities. The Rw value ranges from 0 to 15 and depends on the water pressure, flow rate and chemical activity. Higher values represent drier conditions with low water pressure and flow, while lower values are assigned to wet rock with active water seepage and high pressure (Aziz et al., 2017).

Water present in rock masses can have a significant influence on the bearing capacity of friction anchor bolts used in underground structures. To quantify this impact on the bearing capacity of the bolts, we estimated the water flow rate in the underground structures of the mine using the Rw index of the RMR classification shown in Table 3.

**Table 3:** Parameter of water presence in the RMR index

Inflow per 10m length (l/m)	0	<10	10-25	25-125	>125
Condition	dry	Damp	Wet	Dripping	Flowing
Rw Rating	15	10	7	4	0

To investigate the impact of groundwater presence in imiter rock mass on the load-bearing capacity of cemented bolts, we recorded the pull-out displacements of four bolts installed in four mining sectors (Imiter 1, Imiter 2, ImiterSud, and Igoudrane). These sectors exhibit varying levels of groundwater presence. The four mining zones under study share the same overall rating of RMR=60; however, the rating of the Rw parameter, representing the groundwater presence in the mass, varies across the zones (Figure 14).

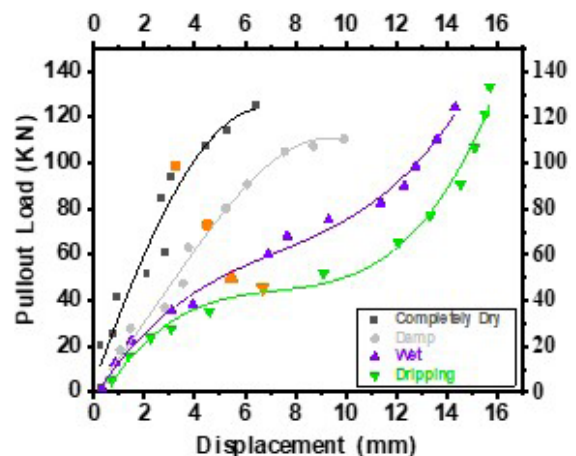


**Fig.14.** Pullout load-displacement with groundwater factor for RMR=60

To establish a correlation between the load-bearing capacity of cemented bolts and the presence of water in the rock mass, we graphically represent the values of the load-bearing capacity as a function of the rating of the  $R_w$  parameter, which characterizes the groundwater presence according to the RMR index (Figure 15).

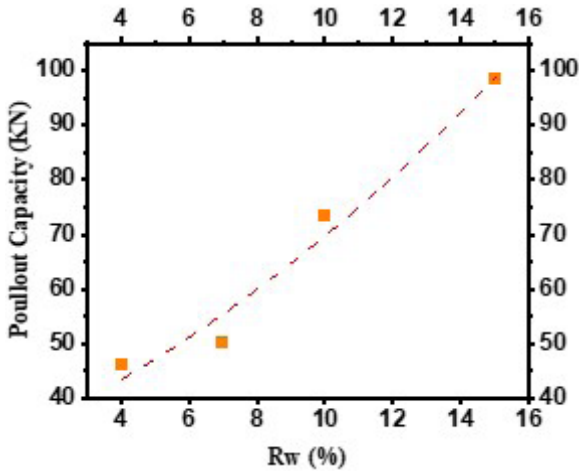


**Fig.15.** Pull-out bearing capacity with groundwater factor for RMR=60

To quantify the correlation between the tensile strength and the  $R_w$  index, the following expression is proposed:

$$BC(KN) = 32,83 e^{0,074 \cdot R_w} ; R^2 = 0,97 \quad (5)$$

The analysis of the results leads to the conclusion that the pull-out load capacity of cemented friction bolts decreases proportionally with the presence of water in the rock mass. Here are some proposed explanations for this impact:

**Reduction of friction:** When water infiltrates into cracks and joints in the rock, it can reduce the friction between the anchor bolt and the rock wall. This can weaken the holding capacity of the bolt, resulting in a reduction in load-bearing capacity.

**Rock erosion:** Water can cause erosion of the surrounding rock, weakening the overall structure of the rock wall. This can decrease the rock's ability to support the load exerted by the anchor bolt, thus reducing its load-bearing capacity.

**Corrosion of the anchor bolt:** Water can also lead to corrosion of the anchor bolt, especially if it is made of steel. Corrosion weakens the bolt, diminishing its strength and load-bearing capacity.

**Rock swelling:** In certain situations, when water penetrates into the rock, it can cause the rock to swell. This swelling can act like a lubricant on the

anchor bolt, thus reducing its load-bearing capacity.

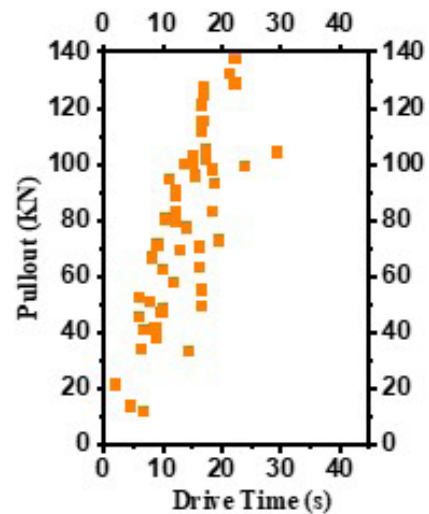
To mitigate the effects of water on the load-bearing capacity of friction anchor bolts, several measures can be taken, such as using corrosion-resistant materials and implementing drainage systems to remove water.

### 3.5 The effect of Rock Bolt-Drilled Hole diametrical difference on pull-out resistance

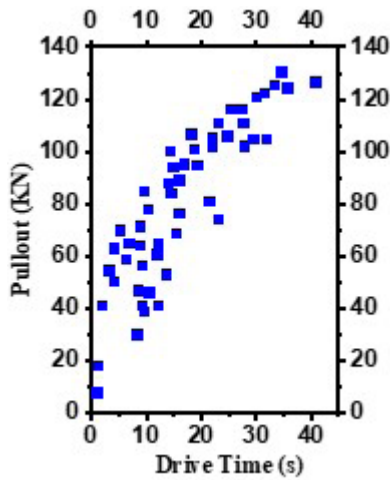
The installation time of rock bolts into boreholes can be used as an indicator of the difficulty encountered by the drilling equipment during the bolt insertion process. This installation time parameter can be linked to Bolt-Hole diametrical difference (BHDD) then be correlated with the force required to extract the rock bolt from the borehole in pull-out testing.

An experimental investigation was conducted to determine the influence of rock bolt installation rate on the pull-out resistance for varying bolt-borehole diametrical differences. The study involved installation of 34 mm, 36 mm, and 38 mm diameter rock bolts into 33 mm diameter boreholes drilled in a rock mass of moderate quality, with an RMR of 60 and Q-value of 5. The insertion time was measured for each bolt diameter and correlated to the maximum pull-out load obtained from extraction testing. The results shown in Figure 16 demonstrate that longer installation times, corresponding to slower drive speeds, lead to higher ultimate pull-out loads for increased diametrical differences between the bolt and borehole diameters examined. Excluding anomalous outliers, a clear trend is observed where slower insertion s, and therefore higher bolt-borehole diametrical differences, produce increased pull-out resistance.

a) BHDD=1mm



b) BHDD=3mm



c) BHDD=5mm

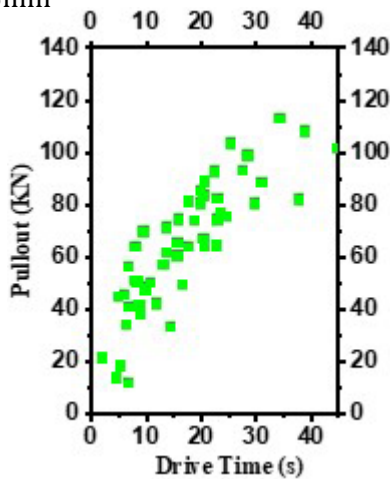


**Fig.16.** Pullout load-displacement with drive time for a)  $D = 34$  mm, b)  $D = 36$  mm and c)  $D = 38$  mm

Results from field pull-out tests demonstrate that the more the drilled hole is smaller than the rock bolt diameter the more the bolt necessitate a longer drive time for placement into the borehole. This increased duration of the rock bolt insertion process for reduced bolt diameters directly relates to an increase in the measured pull-out resistance. This observation suggests that increasing the rock bolt diameter leads to greater friction and mechanical interlock between the bolt and the borehole wall.

The regression curves of the drive time for each Bolt-Hole diametrical difference (BHDD) are given by the following expressions:

$$UC_{(BHDD=1mm)} = 53 \ln(Dt) - 56.3 \quad (6)$$

$$UC_{(BHDD=3mm)} = 32.56 \ln(Dt) - 4 \quad (7)$$

$$UC_{(BHDD=5mm)} = 32.1 \ln(Dt) - 18.7 \quad (8)$$

Overlaying the regression curves of each Bolt-Hole diametrical difference on a single graph provides a clear understanding of the pull-out resistance domains based on the drilling advancement speed (Figure 17).

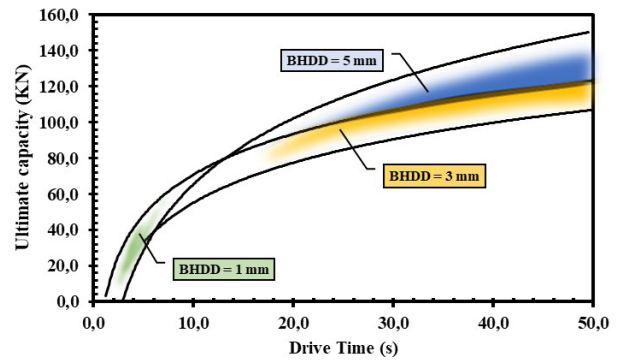


**Fig.17.** Pullout load-displacement with drive time

By utilizing the provided regression equations for the different bolt diameters, it becomes possible to estimate the pull-out resistance based on driving time and Bolt-Hole diametrical difference. This estimation can be used to evaluate bolt performance under specific conditions and make appropriate decisions regarding design and safety.

### 3.6 Impact of Water-to-Cement Ratio on Rock Bolt Resistance

As the water increases in a water-cement ratio, the strength and durability of cured concrete will decrease (Aziz et al., 2017), This is due to an increase in water particles between the cement particles, as the water evaporates over time air will replace the water, leaving the concrete porous (Wong and Buenfeld, 2009). These pores offer little structural support and therefore will reduce the strength of the concrete structure.

The water-to-cement ratio ( $w/c$ ) is the most important factor in concrete mix design as it controls the mechanical properties and durability of hardened concrete. The water-to-cement ratio represents the mass ratio of water to cement in freshly prepared concrete, and it is defined by dividing the amount of water in the mix by the weight of cement, both of which are fixed in the same concrete mix.

$$WCR = \frac{w}{c} \quad (9)$$

A pullout test was conducted on four bolts installed with four different water-to-cement ratios, after 28 days from the date of their installation. In

order to avoid the influence of water presence and the quality of the rock mass, it was decided to install the bolts in dry blocks with an RMR rating of 60 (Figure 18).

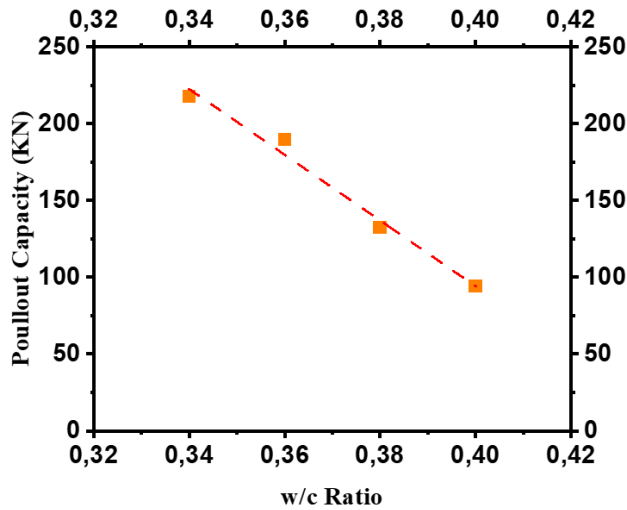


**Fig.18.** Pull-out bearing capacity with WCR ratio (RMR=60; Curing time=28 Days)

We propose the following model:

$$BC_{WCR} \text{ (KN)} = a + b \cdot WCR \quad (10)$$

**Table 3.** Parameter of adjusted linear model

Coefficients	Optimized Values
A	950,7 ± 69,18
B	-2141,5 ± 186,63
R <sup>2</sup>	0,98

Experimentally, a ratio of 0.34 provides the best bolt-rock resistance; however, other issues arise with this ratio. The pumpability of the grout decreases, and several difficulties arise during application. Pumpability increases as the ratio becomes higher, which facilitates the filling of the boreholes. However, this reduces the bond strength.

#### 4. Conclusion

In conclusion, the study demonstrates the effectiveness of cementitious concrete injection in enhancing the bearing capacity of friction anchor bolts and reinforcing their anchorage in underground structures. The injection of a cement-based mixture comprising cement, sand, and additives into the bolt leads to internal expansion, resulting in increased volume and improved frictional interaction between the bolt and the rock mass. The main conclusions and advantages of this method can be summarized as follows:

**Increased Adherence:** The radial force exerted by the expanded concrete enhances the adhesion between the bolt and the rock mass, improving the bolt's ability to resist pull-out forces.

**Enhanced Load Transfer:** The radial force transmitted by the expanded concrete aids in transferring applied loads from the bolt to the rock mass, resulting in reduced local stresses on the bolt and better distribution of forces, thereby enhancing overall pull-out resistance.

**Void Filling:** The expansion of the concrete helps fill voids inside the bolt and between the bolt and the rock, ensuring closer contact between the bolt and the rock. This improves the efficiency of anchorage.

**Overall Stability:** The increase in concrete volume contributes to the overall stability of the support system by reinforcing the bolt anchorage. It reduces undesired movements or deformations of the bolt and rock mass, enhancing the strength and durability of the support structure.

**Silicate-Based additive:** The incorporation of a silicate-based additive accelerates the curing time of the cement, enhancing the strength of the bolts. This allows for immediate support after the injection process.

**Influence of Groundwater:** The study highlights the significant influence of groundwater on the bearing capacity of cemented bolts. It emphasizes the importance of considering groundwater conditions in the design and application of cemented friction anchor bolts.

The pullout tests conducted on various rock masses demonstrate that higher rock mass quality and longer cemented bolts result in increased pullout resistance. The length of the anchorage bolt plays a significant role in the bearing capacity, with longer bolts exhibiting higher tensile strength and pull-out resistance. The proposed empirical equations provide estimates for the bearing capacity based on the rock mass quality and cemented bolt length.

Overall, the cemented concrete injection technique offers a promising approach to enhance the strength and anchorage of friction anchor bolts in underground structures. It provides specific advantages such as increased adhesion, load transfer, and overall stability of the support system. The use of a silicate-based additive accelerates the curing time, further enhancing the strength of the bolts. Considering groundwater conditions is crucial for optimal performance.

While this study demonstrates the potential of cementitious concrete injection to enhance friction anchor bolts, there remains significant scope for further optimization through ongoing research. Comparative analysis against traditional bolting solutions will help refine the technique and quantify potential disadvantages to be mitigated. The installation of hollow split rockbolts requires additional procedural steps compared to traditional bolting methods. These extra operations reduce the pur-

ported technological superiority of split bolts over conventional supports. Moreover, the lower elastic modulus of a cement mortar bolt relative to a hollow bolt may have detrimental effects. The reduced elasticity could lead to worsening of adhesion properties at the bolt-rock mass interface as blasthole diameter enlarges resulting from progressive rock fracture during mining activities. This potential adhesion deterioration and loss of friction should be thoroughly examined.

## References

- Aziz, N., Majoor, D., & Mirzaghobanali, A. (2017). Strength properties of grout for strata reinforcement. *Procedia engineering*, 191, 1178-1184.
- Barton, N., Løset, F., Lien, R., & Lunde, J. (1981). Application of Q-system in design decisions concerning dimensions and appropriate support for underground installations. In *Subsurface space* (pp. 553-561).
- Bieniawski, Z. T. (1973). Engineering classification of jointed rock masses. *Civil Engineering=Siviele Ingenieurswese*,(12), 335-343.
- Bieniawski, Z. (1988). The rock mass rating (RMR) system (geomechanics classification) in engineering practice. In *Rock Classification Systems for Engineering Purposes*. ASTM International.
- Kılıc, A., Yasar, E., & Celik, A. G. (2002) Effect of grout properties on the pull-out load capacity of fully grouted rock bolt. *Tunnelling and underground space technology*, ;17(4), 355-362.
- Komurlu, E., & Demir, S. (2019). Length effect on load bearing capacities of friction rock bolts. *Periodica Polytechnica-Civil Engineering*, 63(3).
- Li, C. C. (2017) Principles of rockbolting design. *Journal of Rock Mechanics and Geotechnical Engineering*; 9(3), 396-414.
- Li, S. C., Wang, H. T., Wang, Q., Jiang, B., Wang, F. Q., Guo, N. B., ... & Ren, Y. X. (2016) Failure mechanism of bolting support and high-strength bolt-grouting technology for deep and soft surrounding rock with high stress. *Journal of Central South University*;23(2), 440-448.
- Liu, J., Li, H., Li, Y., Yang, Y., Sun, T., Song, R., & Sun, R. (2021) Study on the Effect of Isotropic Initial Stress on the Anchoring Performance of Self-Expanding Bolts. *Advances in Civil Engineering*; 1-19.
- Wong, H. S., Zobel, M., Buenfeld, N. R., & Zimmerman, R. W. (2009). Influence of the interfacial transition zone and microcracking on the diffusivity, permeability and sorptivity of cement-based materials after drying. *Magazine of concrete research*, 61(8), 571-589.
- Zhang, Y., Li, X., & Liu, Y. (2017): Numerical simulation of the effect of water-cement ratio on the pull-out resistance of fully grouted rock bolts. *Advances in Civil Engineering* .



## Utilization of wastes/by-products as grinding additives

Serkan Çayırılı<sup>a,\*</sup>, Hasan Serkan Gökçen<sup>b,\*\*</sup>, Nuri Yüce<sup>c,\*\*\*</sup>, Obaidullah Elchi<sup>a,\*\*\*\*</sup>

<sup>a</sup>Niğde Ömer Halisdemir University, Faculty of Engineering, Department of Mining Engineering, Niğde, TÜRKİYE

<sup>b</sup>Eskişehir Osmangazi University, Faculty of Engineering and Architecture, Department of Mining Engineering, Eskişehir, TÜRKİYE

<sup>c</sup>Niğde Ömer Halisdemir University, Graduate School of Natural and Applied Sciences, Department of Mining Engineering, Niğde, TÜRKİYE

Received: 17 August 2023 \* Accepted: 11 October 2023

### ABSTRACT

In this work, the use of water (W) as a grinding additive in addition to waste/by-products such as olive black water (BW) and residue of olive black water (RBW) in calcite dry grinding to be sized in microns was investigated at a laboratory scale. The test results were evaluated in terms of particle size and powder flowability as a function of liquid material dosage and grinding time. The study revealed that the use of any kind of liquid materials tested improved the grinding process compared to the without-aid condition. Removing the water content (RBW) in BW resulted in further improvements in both particle size and powder flowability. The findings from both the BW and W data revealed that the dose increase does not yield favorable outcomes in relation to the fff index. Nevertheless, there was a noticeable enhancement in particle fineness.

**Keywords:** Grinding additive, Waste/by-product, Dry calcite grinding, Powder flowability

### Introduction

With the improvement of technology, micronized calcite (<10 µm) is used as a filler raw material, particularly in sectors such as plastic, paper, and paint. In our country, calcite in micron sizes is manufactured and marketed to the aforementioned industries using dry techniques. In addition to situations where dry processes are mandatory and advantageous (cement, calcite, etc.), the importance of dry processes is increasing with the increasing use of water day by day. It is also important to use dry processes and to increase the studies on this subject, especially in countries where water is limited and in regions where environmental sensitivity is important. Dry grinding additives are one of the subjects on which important studies have been carried out recently in dry grinding. With the increase in the surface area

of the material in dry grinding processes (especially in micronized grinding), intermolecular attraction forces and regional forces and particle-particle interaction increase, and this leads to a change in the flow properties of the material. In dry grinding, this situation is tried to be kept under control with grinding additive chemicals. In the reported studies, the use of pure and commercial chemicals was carried out and their positive influences were presented (Paramasivam and Vedaraman, 1992; Katsioti et al., 2009; Zhang et al., 2015; Gökçen et al., 2015; Toprak et al., 2018; Çayırılı, 2018; Çayırılı, 2022). Also employed as grinding additives were several waste materials and by-products (Gao et al., 2011; Leoneti et al., 2012; Li et al., 2015; Akar and Canbaz, 2016; Li et al., 2016; Zhang et al., 2016; Li et al., 2017; Li et al., 2018; Çayırılı et al., 2020).<sup>1</sup>

\*Corresponding author: sÇayırılı@ohu.edu.tr • <http://orcid.org/0000-0003-3348-6601>

\*\* sGökçen@ogu.edu.tr • <https://orcid.org/0000-0001-5093-6796>

\*\*\*nuri.yuce1000@gmail.com • <https://orcid.org/0000-0001-6953-9053>

\*\*\*\*ubeydullah.elci@gmail.com • <https://orcid.org/0000-0002-5996-5988>

In particular, these chemicals create an extra cost as they are used extensively in grinding processes. Accordingly, the utilization of waste materials or by-products as a grinding additive can be considered as an alternative. Starting from this, the possibility of using olive black water (BW) as a grinding additive in the dry micronized grinding of calcite was investigated. In addition, distilled water (W) and residue of olive black water (RBW) were tested in order to better demonstrate the effectiveness of BW, and comparisons were performed with W and RBW. The grinding experiments were evaluated in terms of particle size and powder flowability as a function of liquid material dosage and grinding time.

## 1. Materials and Methods

### 1.1. Materials

For the dry grinding experiments, a calcite sample (98.838% CaCO<sub>3</sub>) by Mikron'S Inc., Türkiye with a median particle size of x<sub>50</sub>: 83.77 µm was used. Its specific gravity was found to be 2.71 using a helium pycnometer.

In the previously reported study (Çayırılı et al., 2023), the effect of BW on calcite grinding was investigated along with various grinding additives. In order to reveal the effect of BW in more detail, the research was continued, and the distilled water and residue of olive black water were added to the agenda and constituted the main subject of this study. In this context, three liquid materials (BW, W and RBW) were used as grinding additives. Distilled water was preferred in terms of representing the water part of BW. The BW sample was collected from Dalan Oil Industry Inc. in Türkiye. The values of free fatty acids, specifically in terms of oleic acid, in BW, were determined by the analyses made in the Food Engineering Laboratory of Niğde Ömer Halisdemir University. In this context, free fatty acidity values were found to be 2-3%. In order to increase the fatty acid concentration in BW and to observe the influences of the water in it on the experimental results, RBW was obtained by evaporating 84% of the water in the BW content at 100°C.

### 1.2. Methods

The grinding experiments were conducted using a vertical batch-type laboratory stirred ball mill (Figure 1). As introduced in a former study (Çayırılı et al., 2023), the mill is equipped with a cylindrical 1200 ml grinding chamber made of steel and equipped with a water jacket. Both, shaft and stirrers (pin type) are also made of stainless steel. After weighing the samples and balls in accordance with the test conditions, the balls were fed first into the grinding chamber, and

then the sample was placed second. The liquid material was added to the calcite sample. The shaft was placed into the chamber by adjusting the speed of the agitator to ~100 rpm. After all the settings of the mill were made, the cap was sealed, the planning speed was set, and the milling operation began. The mill was stopped at the determined grinding time. Experimental conditions are summarized in Table 1 and related calculations are given in Equation (1), (2) and (3). At the end of the experiment, the mill cap was opened first and the material and balls were removed from the grinding chamber and their separation was made by sieving. According to sample division techniques, representative samples from the obtained products were taken for size and flowability measurements.



**Figure 1.** Vertical batch-type laboratory stirred ball mill, pin-type stirrer and grinding tank

**Table 1.** Test conditions for dry grinding (Çayırılı, et al., 2023)

Parameter	Value
Stirrer velocity (m/s)	4
Ball loading (J*)	0.60
Powder-ball loading (U*)	0.80
Liquid material dosage (g/t)	0, 500, 1000, 2000, 4000
Ball diameter (mm)	2.8-3.2 (average 3)
Density of ball (g/cm <sup>3</sup> )	~3.7
Milling time (min)	5.5, 7.5, 9.5

$$*J = \frac{\text{mass of balls/ball density}}{\text{mill volume}} \times \frac{1.0}{0.60} \quad (1)$$

$$*fc = \frac{\text{mass of powder/powder density}}{\text{mill volume}} \times \frac{1.0}{0.60} \quad (2)$$

$$*U = \frac{fc}{0.40J} \quad (3)$$

The particle size distributions of the product samples were measured by laser diffraction using Malvern 2000 Ver. 2.00 with Hydro 2000 MU attachment (Malvern Co., Ltd., UK). The device repeats the measurement of each sample at certain intervals and measures three times and gives the average of these three measurements.

The powder flowability was analyzed using a ring shear tester (230VAC-Brookfield, UK) (Figure 2). The sample cell of the device (230 cm<sup>3</sup>, 6in diameter) consists of a movable upper disc and a still lower chamber. In the upper disc, there are 18 chambers in order to create shear stress in the powder whose flowability is desired to be measured. The lower chamber is designed as a perforated plate to prevent the sliding movement of the powder material on the surface. While the lower chamber is stationary, the upper disc applies consolidation stress ( $\sigma_1$ ) at varying rates with downward linear movement and at the same time causes unconfined yield strength in the powder sample with its rotational movement. The basic measurement principle of the powder flow tester is based on measuring the powder material's necessary shear stress ( $\sigma_c$ ) to begin to flow or deform after the compression stress is applied (Slettengren et al., 2015; Çayırılı et al., 2023). At this point, the flowability index  $ff_p$ , which is defined as the ratio between consolidation stress  $\sigma_1$  and unconfined yield strength  $\sigma_c$  (see Equation 4), is used to qualify the powder flowability:

$$ff_p = \frac{\sigma_1}{\sigma_c} \quad (4)$$

Powder flowability can be categorized using the  $ff_p$  value, according to Jenike (1964). In the range  $ff_p < 1$ ,  $1 < ff_p < 2$ ,  $2 < ff_p < 4$  and  $4 < ff_p < 10$ ,  $10 < ff_p$  a powder is non-flowing, very cohesive, cohesive, easy-flowing and free-flowing, respectively.



Figure 2. Powder flow tester

## 2. Results and Discussion

### 2.1. Comparison in terms of product fineness

The influence of the liquid material type and its level of concentration on the fineness of the product was examined by wet particle size measurements, as depicted in Figure 3. Without aid conditions, particle sizes of 8.05, 7.49, and 6.18  $\mu\text{m}$  were obtained at grinding times of 5.5, 7.5, and 9.5 min, respectively. Regarding BW, there is a lack of significant impact on the  $d_{50}$  value when the additive concentration is low and the time to grind is 5.5 min, compared to when there are no additives. In contrast, it has been noticed that the use of BW results in a significant enhancement in the  $d_{50}$  size at concentrations of 1000 and 2000 g/t. Higher BW dosing (4000 g/t) resulted in poor grinding performance. This result can be explained by the fact that as the amount of BW increases, the amount of water in the sample concentrate also increases. Because there is a high amount of water in BW. Additional water dosing (liquid bridging) generates forces of adhesion that are relatively strong, which in turn raises powder cohesion (Rumpf, 1974). Moreover, for each evaluated grinding time, the positive impact of BW at concentrations of up to 4000 g/t was seen. The results also showed that the  $d_{50}$  sizes decreased from 7.92 to 6.31  $\mu\text{m}$  when BW was increasing at dosages ranging from 500 g/t to 2000 g/t at a shorter milling period as opposed to the without-aid condition, which had an 8.05  $\mu\text{m}$   $d_{50}$  value at a 5.5 min grinding time as already shown in the former study (Çayırılı et al., 2023).

In comparison to the without-aid condition, the  $d_{50}$  size was reduced with increasing RBW dosage for each milling period of time. In addition, as the grinding time increased, the use of more RBW resulted in finer particle size. In other words, at each grinding time, the effect of the RBW dosage was observed.

In the case of using water, the  $d_{50}$  size did not change (compared to the without-aid condition) for the short grinding time (5.5 min) as its dosage increased. As the grinding time increased, the  $d_{50}$  size decreased, particularly at a 1000 g/t dosage. Further dosing (2000 g/t) adversely affected the milling performance. It was also determined by Toraman et al. (2016) that the increasing concentration of water has a negative effect on grinding. In their work, they investigated how water affects particle fineness and surface area, indicated that it had a positive effect on grinding performance up to a certain amount and observed that the administration of higher dosages resulted in a negative impact.

Consequently, in 5.5 min grinding experiments using BW, the finest particle size,  $d_{50}$ : 6.31  $\mu\text{m}$ , was obtained by using 2000 g/t BW. Similarly, a particle size of  $d_{50}$ :5.94  $\mu\text{m}$  was attained using a dosage of 2000 g/t RBW, also within a 5.5 min grinding duration. Additionally, W achieved a particle size of  $d_{50}$ :7.71  $\mu\text{m}$  at 1000 g/t in 5.5 min experiments. At the end of the grinding process lasting 7.5 min, the most refined particle sizes were achieved with  $d_{50}$  values of 5.79 and 5.75 when utilizing 2000 g/t in BW and RBW, respectively. However, a  $d_{50}$  value of 6.61 was obtained at a concentration of 1000 g/t when employing W. Within the experiments, the longest grinding time utilized was 9.5 min, resulting in the acquisition of the finest particle sizes when employing a dosage of 2000 g/t for both BW and RBW. The particle sizes acquired are 5.34 and 4.82  $\mu\text{m}$ , respectively. The utilization of W resulted in the attainment of the particle size  $d_{50}$ :5.42  $\mu\text{m}$  at a concentration of 1000 g/t.

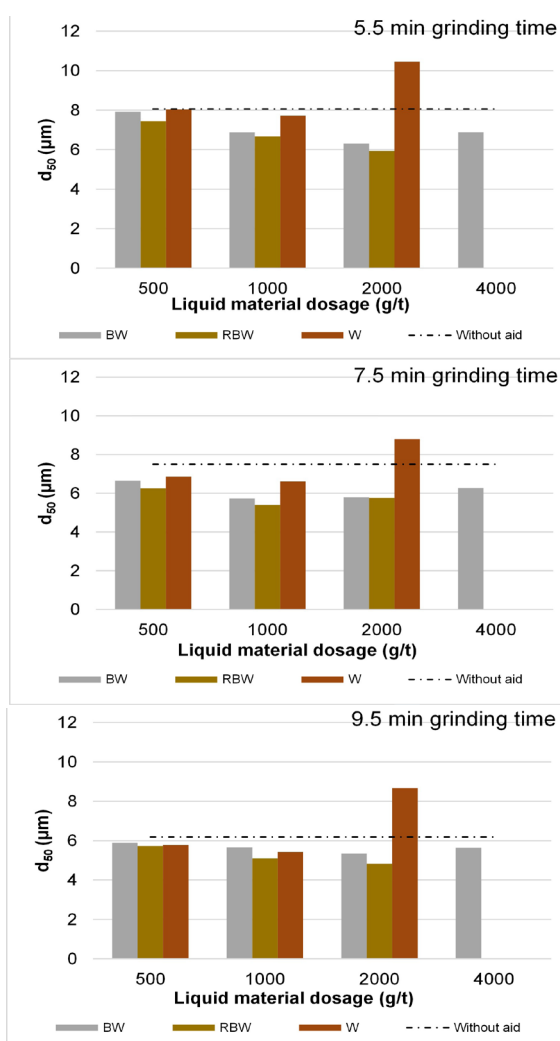


**Figure 3.** The influence of all tested liquid materials on particle size

## 2.2. Comparison in terms of powder flowability

The impact of liquid materials on the flowability of powders is depicted in Figure 4, which presents the  $ff_p$  indices of the product powders. Among the all investigated liquid materials, only RBW affected the powder flowability compared to the without-aid condition. As the grinding time increased, the use of more RBW resulted in finer particle size. It can be said that the influence of RBW dosage is demonstrated at every milling time. Surprisingly, the BW and W powder flowabilities were lower than the results from the without-aid condition. To put it another way, the data from BW and W indicated that the  $ff_p$  index would not benefit from the dosage increase.

Although the use of water and BW has an influence on the size, they do not cause any change in the powder flowability, an indication that the positive influence on grinding cannot only be explained by the powder flowability. Prziwara et al. (2018) also examined the effects of different types of grinding aids on grinding performance and powder flowability and determined that some of them had positive effects on particle size, although they did not have a positive effect on agglomeration and powder flowability.

In terms of powder flowability values, 2.08, 1.92 and 1.81  $ff_p$  values were obtained in the 5.5, 7.5 and 9.5 grinding time experiments, respectively, in the condition where without grinding aid was used. In 5.5 min, grinding time experiments, the highest fluidity values for BW, RBW and W were achieved when 2000 g/t was used, and 1.81, 2.43 and 1.78  $ff_p$  values were obtained at this amount, respectively. During the experiments with a grinding time of 7.5 minutes, it was observed that the maximum  $ff_p$  value in BW was 1.61 at a concentration of 500 g/t. Similarly, the highest  $ff_p$  value in RBW was 2.22 at a concentration of 1000 g/t. Additionally, the highest  $ff_p$  value in W was recorded as 1.75 at a concentration of 2000 g/t. Finally, during the experiments with a grinding time of 9.5 min, it was observed that the maximum  $ff_p$  value in BW was 1.78 at a concentration of 4000 g/t. Similarly, the highest  $ff_p$  value in RBW was 2.00 at a concentration of 2000 g/t. Additionally, the highest  $ff_p$  value in W was recorded as 1.72 at a concentration of 2000 g/t.

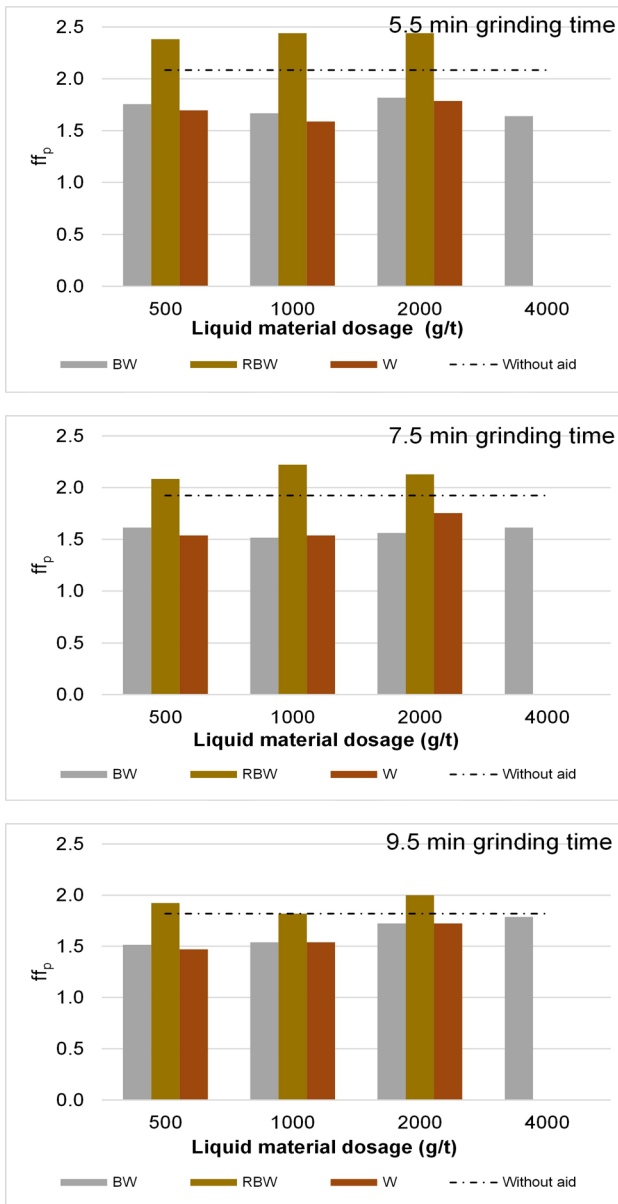


**Figure 4.** The influence of all tested liquid materials on  $ff_p$  index

To better determine the effectiveness of BW, distilled water experiments to represent the water part of the olive black water and residue experiments to represent the main substance group were carried out. According to these results, it has been revealed that RBW is more effective than W and BW in terms of particle size. According to these results, it has been revealed that the RBW is more effective than W and BW in terms of product fineness. In addition, it was found that the  $ff_p$  values overlapped with the particle size results. In other words, BW is worse than RBW and better than W in terms of flowability/grinding performance. However, BW having high water content, reduced the fluidity of the product

(according to the without-aid condition), unlike RBW. It is thought that this finding is caused by the substance group increasing the powder flowability (residue-free fatty acidity 2-3%). Studies from the scientific literature can be presented as evidence for this comment. Paramasivam and Vedaraman (1993) investigated the effect of six types of fatty acids (stearic acid, lauric acid, palmitic acid, sodium lauryl sulfate, calcium stearate, and magnesium stearate) on the dry grinding of calcite. According to the findings of this study, it was determined that the fineness, bulk density and packaged bulk density of the milled product increased with the use of any tested fatty acid, while the compressibility and tensile strength of the powder bed of the milled product decreased. The reason for the change in these flow characteristics inside the mill was the adsorption of the tested long-chain fatty acid molecules on the particle surfaces, reducing the friction forces and adhesion interactions between them. In another study, the grinding performance of fatty acids (capric acid, lauric acid, myristic acid, palmitic acid, and stearic acid) used in grinding chitosan powder in a vibrating mill was examined according to fatty acid length. According to the results, it was determined that all fatty acids tested improved the grinding performance compared to the condition without grinding aid, and the best performance was obtained with stearic acid (having the longest carbon chain) (Fukumori et al., 1998). BadJena and Mishra (2011), in their study, found that stearic acid is a better grinding aid than paraffin wax and oxalic acid in grinding brass powder. Ma et al. (2013) also examined the effect of oleic acid in grinding cement. The results showed that the use of oleic acid improved the surface area and especially the rheological properties of the cement.

On the other hand, some sources from the literature confirm that water can indeed increase grinding efficiencies (Parks, 1984; Sohoni et al., 1991; Sverak et al., 2013; Çayırılı, 2014; Toraman et al., 2016; Prziwara and Kwade, 2020). As is commonly known, water molecules have a significant polar attraction, which results in relatively strong affinities for polar regions on the solid surface, similar to the polar functional groups found in conventional grinding additive molecules, hence lowering intergranular adhesion forces (Prziwara et al., 2018; Prziwara and Kwade, 2020). Parks (1984) observed in his research that it reduces the surface energy

between quartz particles. In parallel with these comments, in the current investigation, it may be assumed that BW (with the existing water content) created a grinding environment by reducing the flowability in the grinding chamber which will enable the particles to be stressed more effectively by the balls. Thus, in light of the findings and comments obtained with BW in the current study, it is thought that both the residue part and the water part contribute to the grinding separately.

### 3. Conclusion

Experimental studies on grinding performance using calcite in a stirred ball mill have been carried out. The influences of liquid materials used as a grinding additive (olive black water, distilled water and residue of olive black water) on the particle size and powder flowability were examined. The dry grinding experiments and analyses showed that:

- The study revealed that using any of the liquid materials evaluated enhanced the grinding process

### Acknowledgements

The authors would like to thank The Scientific and Technological Research Council of Turkey (Grant No. 119M216) for the financial support of

### References

Akar, C., Canbaz, M. 2016. Effect of molasses as an admixture on concrete durability. *Journal of Cleaner Production*. 112, 2374-2380.

BadJena, S.K. Mishra, B.K. 2011. Optimization of variables in grinding brass particles for paint and pigment industry. *Powder Technol.* 214,349-355.

Çayırılı, S. 2018. Influences of operating parameters on dry ball mill performance. *Physicochemical Problems of Minerals Process.* 54, 751-762.

Çayırılı, S. 2022. Analysis of grinding aid performance effects on dry fine milling of calcite. *Advanced Powder Technology.* 33, 103446.

Çayırılı, S., Gökçen, H. S., Yüce, N., Elchi, O. 2023. Investigation of the usage of waste materials and by-products as grinding aids in calcite grinding. *Minerals Engineering.* 202, 108267.

Çayırılı, S. 2014. Investigation of the effects of grinding parameters on mica grinding in a stirred ball mill. Ph. D. Thesis (In Turkish). Eskişehir: Eskişehir Osmangazi University.

versus the without-aid condition.

- In other words, at the longest grinding time tested,  $d_{50}$  values of 5.42, 5.34, and 4.82  $\mu\text{m}$  were reached at certain concentrations W, BW, and RBW, respectively, whereas a product with a  $d_{50}$  size of 6.18  $\mu\text{m}$  was obtained at the without-aid condition.

- Considering RBW, powder flowability improved as liquid material concentration increased. Namely, while  $ff_p$  values varied between 1.81 and 2.08 in the without-aid condition, the flowability index of the products obtained with the use of RBW increased from 1.81 to 2.43. Surprisingly, the BW and W findings showed that the rise in concentration was not advantageous regarding the  $ff_p$  values; however, the improvement in particle fineness was clear.

- Removing the water content (RBW) in BW resulted in further improvements in both particle size and powder flowability.

- Finally, it can be concluded that both the residue part and the water part of BW contribute to the grinding separately.

this research project. Additionally, the authors express their gratitude to Mikron'S Inc. for supplying the calcite samples and to Dalan Chemistry for the provision of black water.

Çayırılı S., Gökçen, H. S., Yüce, N., Elchi, O. 2020. The investigation of usability of olive pomace oil as a grinding aid. *Journal of Engineering and Architecture Faculty of Eskişehir Osmangazi University.* 29(2), 189-201.

Fukumori, Y., Tamura, H., Jono, K., Miyamoto, M., Tokumitsu, H., Ichikawa, H., Block, L.H. 1998. Dry grinding of chitosan powder by a planetary ball mill. *Adv. Powder Technol.* 9, 281-292.

Gao, X., Yingzi, Y., Hongwei, D. 2011. Utilization of beet molasses as a grinding aid in blended cements. *Construction and Building Materials.* 25, 3782-3789.

Gökçen, H. S., Çayırılı, S., Ucbas, Y., Kayaci, K. 2015. The effect of grinding aids on dry micro fine grinding of feldspar. *International Journal of Mineral Processing.* 136(Supplement C), 42-44.

Jenike, A.W. 1964. Storage and Flow of Solids, *Bull. Utah Eng. Exp. Station* 123.

- Katsioti, M., Tsakiridis, P. E., Giannatos, P., Tsibouki, Z., Marinos, J. 2009. Characterization of various cement grinding aids and their impact on grindability and cement performance. *Construction and Building Materials*. 23(5), 1954-1959.
- Leoneti, A. B., Aragão-Leoneti, V., Oliveira, S. V. W. B. 2012. Glycerol as a by-product of biodiesel production in Brazil: Alternatives for the use of unrefined glycerol. *Renewable Energy*. 45, 138-145.
- Li, H., Jiang, Z., Yang, X., Yu, L., Zhang, G., Wu, J., Liu, X. 2015. Sustainable resource opportunity for cane molasses: use of cane molasses as a grinding aid in the production of Portland cement. *Journal of Cleaner Production*. 93, 56-64.
- Li, H., Zhao, J., Huang, Y., Jiang, Z., Yang, X., Yang, Z., Chen, Q. 2016. Investigation on the potential of waste cooking oil as a grinding aid in Portland cement. *Journal of Environmental Management*. 184, 545-551.
- Li, L., Feng, Y., Liu, M., Zhao, F. 2017. Preparation of grinding aid using waste acid residue from plasticizer plant. *International Conference on Materials Sciences and Nanomaterials*, 230.
- Li, W., Ma, S., Shen, X. 2018. Washington Patent No. 10,077,211. U.S. Patent and Trademark Office.
- Ma, B., Wang, J., Li, X., He, C., Yang, H. 2013. The influence of oleic acid on the hydration and mechanical properties of Portland cement. *J. Wuhan Univ. Technol. Mater. Sci.* 28(6), 1177-1180.
- Paramasivam, R., Vedaraman, R. 1992. Effects of the physical properties of liquid additives on dry grinding. *Powder Technology*. 70(1), 43-50.
- Paramasivam, R., Vedaraman, R. 1993. Effect of fatty acid additives on the material flow properties of dry grinding. *Powder Technol.* 77, 69-78.
- Parks, G. A. 1984. Surface and interfacial free energies of quartz. *J. Geophys. Res.* 89, 3997-4008.
- Prziwara, P., Breitung-Faes, S., Kwade, A. 2018. Impact of grinding aids on dry grinding performance, bulk properties and surface energy. *Advanced Powder Technology*. 29(2), 416-425.
- Prziwara, P., Kwade, A. 2020. Grinding aids for dry fine grinding processes – Part I: Mechanism of action and lab-scale grinding. *Powder Technology*. 375, 146-160.
- Rumpf, H. 1974. Die Wissenschaft des Agglomerierens. *Chem. Ingenieur Technik*. 1, 1-11.
- Slettengren K, Xanthakis E, Ahrné L, Windhab EJ. 2015. Flow properties of spices measured with powder flow tester and ring shear tester-XS. *Int. J. Food Prop.* 19, 1475-1482.
- Sverak, T. S., Baker, C. G. J., Kozdas, O. 2013. Efficiency of grinding stabilizers in cement clinker processing. *Minerals Engineering*. 43-44, 52-57.
- Sohoni, S., Sridhar, R., Mandal, G. 1991. The effect of grinding aids on the fine grinding of limestone, quartz and portland cement clinker. *Powder Technology*. 67(3), 277-286.
- Toprak, N. A., Altun, O., Benzer, H. 2018. The Effect of grinding aids on modelling of air classification of cement. *Construction and Building Materials*. 160, 564-573.
- Toraman, O.Y., Çayırılı, S., Ucurum, M. 2016. The grinding-aids effect of moisture, triethanolamine (tea) and ethylene glycol (eg) on grinding performance and product quality of calcite. *International Journal of Engineering Research & Science (IJOER)*. 2(12), 121-128.
- Zhang, T., Gao, J., Hu, J. 2015. Preparation of polymer-based cement grinding aid and their performance on grindability. *Construction and Building Materials*. 75, 163-168.
- Zhang, Y., Fei, A., Li, D. 2016. Utilization of waste glycerin, industry lignin and cane molasses as grinding aids in blended cement. *Construction and Building Materials*. 123, 785-791.





## Dust pollution characteristics and control measures of open cut coal mines

Leng Wu<sup>a\*</sup>, Ziling Song<sup>b\*\*</sup>

<sup>a</sup>College of Mining, Liaoning Technical University, Fuxin 123000, CHINA

<sup>b</sup>College of Environmental Science and Engineering, Liaoning Technical University, Fuxin 123000, CHINA

Received: 28 July 2022 \* Accepted: 16 October 2023

### ABSTRACT

This paper provides a study on dust pollution in open cut coal mines and related characteristics and emission prevention measures. Dust laden soil samples were collected from open cut coal mines and subjected to alkaline digestion testing to determine the content of heavy metal pollutants and total pollutants. Then, the physical and chemical properties of the soil samples were measured and analysed. The effects of different phosphorus treatments on the pH value and water-soluble phosphorus of dust laden soil samples, as well as the content of water-soluble lead, zinc, and exchangeable lead and zinc in the soil samples were investigated. On this basis, multi-directional dust pollution control measures with public participation in construction dust supervision and control as the core are put forward. The test findings demonstrate that after the treatment, the amount of dust is decreased, the contaminated open cut coal mines soil may be repaired, and a satisfactory soil remediation impact is achieved. This study helps with the green and sustainable development in the area of intelligent coal mines and is a useful resource for addressing the issue of dust pollution in open cut coal mines.

**Keywords:** Open cut coal mines; Dust pollution characteristics; Management measures; Water soluble; pH value; Containing substance

### Introduction

Although coal is still the largest source of primary energy consumption in all countries, the influence of environmental protection factors such as haze has led many countries to introduce coal restriction policies (Meha *et al.*, 2020). Coal industry is one of the important sources of global energy production and consumption, but it is also one of the main pollution sources of environmental pollution and resource waste (Jiskani *et al.*, 2021). This is mainly because coal mining will produce dust, waste gas, waste water, solid waste and other pollutants which could have a serious impact on the mining environment and public health. Therefore, the coal industry needs to take measures to reduce the emissions of these pollutants to protect the environment and public health. At the same time, the coal industry also needs to improve energy efficiency, increase operational efficiency, and address environmental and energy challenges such as climate change. In the future, the coal industry must develop towards green mining and

clean utilisation to achieve sustainable development (Jiskani *et al.*, 2022). In the coal industry, coal production capacity is controlled by means of annual working hours and output targets, and coal mines with low safety levels and high production costs are closed, mainly open cut coal mines. The reasons are multifaceted: open cut coal mines have a high level of safety and fewer serious casualties; Low production cost of open pit coal mines, adapting to the current industry downturn situation; The production of open cut coal mines is easy to control and can respond to changes in market supply and demand relationships (Coglianese *et al.*, 2020). It is expected that the output of open cut coal mines will further increase in the proportion of the total domestic coal output (Trechera *et al.*, 2021). The new open cut coal mines pay more attention to water shortage areas, where there are many rocks, dry soil, less rain, and some areas may also encounter sandstorms. In open areas, coal mines are more likely to produce a large amount of dust during mining. Therefore, the calls

\*Leng WU wuleng999@163.com <https://orcid.org/13591000480.0000-0001-9606-0953>

\*\*Ziling SONG abq74295813@126.com <https://orcid.org/15236859563.0000-0001-7130-9185>

<https://doi.org/1030797/madencilik.1149989>

for environmental protection from the entire society is increasing, mostly for controlling coal production and consumption, especially for the coal mines that cause environmental pollution. This requires that dust emissions must be controlled externally during the production and use of coal (Jing *et al.*, 2021). Studying the mechanism and laws of the occurrence, accumulation, migration, and diffusion of dust in open-out mines is a necessary link for the development of green mining in this area. This has certain guiding significance for dust control and dust reduction in open-pit mines.

In recent studies on dust emissions, Luo *et al.* (2021) studied the problem of PM concentration in hawusu open cut coal mine, and analysed the characteristics of PM changes and its relationship with meteorological factors. The average PM concentrations in the study area were lower than the average daily limit of China's national ambient air quality standard (GB 3095-2012). However, the average PM10 concentration in December exceeded the national limit value. The order of PM concentration was December > January > February. Among them, PM concentration was positively correlated with humidity and negatively correlated with wind speed. In December, temperature was positively correlated with PM concentration, while in January, temperature was negatively correlated with PM concentration. Therefore, under the combined effect of several meteorological factors, the order of influence on winter PM concentration at the bottom of the open pit is: humidity > temperature > wind speed > temperature difference. The findings of this study are helpful for green mining. Wang *et al.* (2022) investigated the dust pollution of open cut coal mines in cold areas and explored the main causes and influencing factors. The study determined the characteristics of dust pollution through statistical analysis and calculated the main factors affecting dust concentration using the comprehensive gray correlation. The results show that meteorological factors with significant effects on dust concentration vary by season, including dew point temperature in spring, solar radiation in summer and autumn, and boundary layer height in winter. Winter, followed by autumn and spring, is the most polluting season for mining activities. Based on the study findings, optimal mine design strategies can be developed to reduce dust pollution in mining and adjacent areas. Ding *et al.* (2019) proposed

the effect of viscosity of polymer stabilizer on the structural strength and dust pollution resistance of red sand. The higher the solution viscosity is, the better the crust strength and dust corrosion resistance of red sand surface are. Therefore, the viscosity of polymer solution can effectively predict the structural strength of crust and the ultimate erosion resistance of sand after treatment. Heidari *et al.* (2021) proposed a quantitative source allocation and ecological health risk assessment of heavy metal pollution in urban and heavily polluted suburban road dust. They also analyzed the sources of heavy metals (As, Cd, Co, Cr, Cu, Mn, Ni, Pb, and Zn) in road dust from Abbas City and its western suburbs in Iran, and evaluated their ecological and health risks. Although this study did not analyze the comprehensive factors, it emphasized the attention to traffic emission, which proved that traffic emission was the main source of heavy metals in road dust in the suburbs of Banda Abbas. Therefore, the characteristics and prevention measures of dust pollution in open cut coal mines were put forward, and effective conclusions were drawn. Through the summary of the above research, it can be found that the problem of dust pollution in open cut coal mines is relatively serious, and its harm level is far higher than other pollution sources in industrial production. Therefore, it is necessary to conduct further research on the dust pollution problem in open cut coal mines. After analyzing the characteristics of dust pollution in open cut coal mines, the study proposed some effective prevention and control measures, aiming to provide reference for relevant research.

### **1.1. Comprehensive influence characteristics of dust pollution on atmospheric environment in open cut coal mine**

#### **Dust Pollution Structure in Open Cut Coal Mines**

In the field of modern environmental research, open cut coal mines dust mainly refers to all solid particles that can be suspended in the air for a long time in the area. The particle size range is generally 1-100  $\mu\text{m}$ . According to the size expansion space of 10 $\mu\text{m}$ , the dust of open cut coal mines can be further divided into falling dust or fugitive dust (Markovi *et al.*, 2021). Polluting dust generated during the construction of open cut coal mines is mainly the pollution dust of medium-sized particles with a particle size of about 65  $\mu\text{m}$ , which is the most important source of environmental dust pollution in open cut

coal mines (Benitez-Polo and Velasco, 2020). Dust sources can be divided into topsoil stripping dust and dust generated during production processes, such as mining equipment operations, transportation operations, dumping sites, and coal processing and storage in mining areas. The detailed proportion is shown in Figure 1.

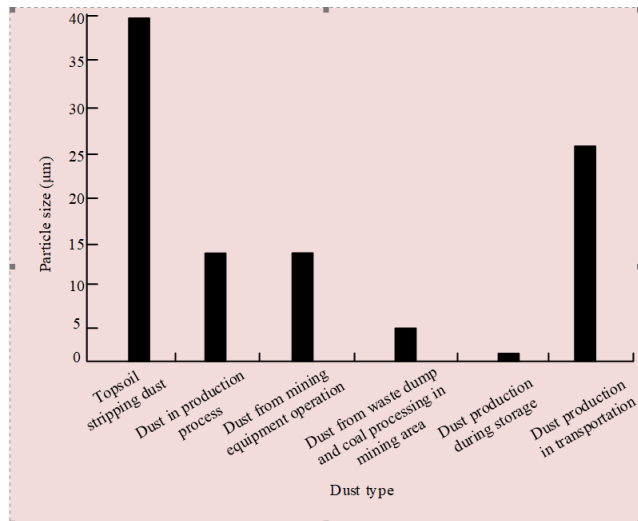


**Figure 1.** Particle size distribution of atmospheric dust from various sources in open cut coal mines

The high-precision definition of dust range in open cut coal mines plays an obvious role in the control of modern urban environmental dust pollution (Ma *et al.*, 2020). The traditional field of surface coal mine dust research has confused industrial dust with domestic dust. This has tended to lead to the definition of the hazards of dust pollution in industry, especially in surface coal mining projects. As a result, the hazards of dust pollution to the atmospheric environment and human health have been grossly underestimated and control methods have lacked real effectiveness. According to the specific characteristics of different dust and signs, such as physical properties, composition, particle size, etc., dust in open cut coal mines can be reasonably classified (Finke *et al.*, 2020; Tong *et al.*, 2019).

## 1.2.Characteristics of Influence of Dust Pollution on Air Environment in Open Cut Coal Mines

The mining sequence of open cut coal mines determines that some coal seams are in an exposed or semi exposed state. The coal seam undergoes a slow oxidation reaction after being exposed to oxygen, and the heat generated accumulates in the coal temperature under conditions where effective diffusion cannot be achieved. When the temperature

rises to the point of coal seam combustion, coal will undergo spontaneous combustion (Guo *et al.*, 2021; Kazi *et al.*, 2019). The combustion process is often inadequate and produces a large amount of smoke and dust, as shown in Figure 2.



**Figure 2.** Smoke dust produced by spontaneous combustion of coal seam

The statistical value and experience of dust emission from dust sources in various links such as drilling, blasting, loading, hauling and drainage of open cut coal mines are shown as follows:

### (1) Drilling

At present, the rotary drilling is mostly used in open cut mines, and the wet dust removal is used. The dust emission of the rotary drill is 1.05 kg/(unit·h) on average according to the field measurement. Some equipment with good dust removal effect can reach 0.22 kg/(set·h).

### (2) Blasting

The amount of dust generated during blasting operation is large, and is affected by different charging methods, blasting mesh methods, and initiation sequences. There are two feasible evaluation methods. One is to establish a monitoring system in the mine to observe the smoke and dust during and after blasting; The Salingermann series method is used to calculate the average concentration of smoke and dust, and the ray recovery method is used to obtain the volume of smoke and dust, thereby calculating the amount of dust. Second, the amount of dust produced by blasting is about 0.0011% of the amount of blasting. The error of the second method is large, so the result can only be used to estimate the order of magnitude.

### (3) Loading

The dust generated during truck and shovel loading operations, and the amount of dust generated can be calculated by the following equation (Wirth et al., 2020):

$$Q_m = Y_n \times D_f \times S_c \times E_v \quad (1)$$

Where,  $Q_m$  is the dust emission intensity [kg/h],  $Y_n$  is the ambient wind speed [m/s],  $D_f$  is the unloading height of the shovel [m],  $S_c$  is the moisture content of the material [%].  $E_v$  is the loading capacity per unit time [ $m^3/h$ ].

### (4) Transportation

The dust produced by railway transportation is small, while the belt conveyor transportation can be controlled by the construction of belt corridor, but the dust in truck haulage is not only large, but also difficult to control. At present, the mainstream of most open cut mines is truck transportation, which is responsible for approximately 60% of the total dust generation in open cut mines. The dust emission from a single truck can be calculated as follows:

$$Q_r = F_b \times H_e \times J_z \quad (2)$$

Where,  $Q_r$  is the dust emission of a single truck [kg/km];  $F_b$  represents the truck running speed, the unit is km/h;  $H_e$  represents vehicle load with unit t;  $J_z$  represents the amount of road surface material, and the unit is  $km/m^2$ .

### (5) Soil dumping link

The dust generated during dumping operations includes unorganized dust generated during truck dumping operations and when the dumping site is exposed to the air and blown by the wind. The former can be calculated according to equation (1), but the latter dominates in the total dust emission. However, the amount of dust raised is directly related to the implementation of greening and reclamation operations in the waste dump, and there is currently no unified formula.

## 2. Experimental analysis

### 2.1. Materials and methods

#### (1) Collection of soil samples from opencast coal mine dust pollution

In the process of setting up sampling points for dust contaminated soil in open cut coal mines, full consideration should be given to the land in front of the chromium slag pile in the research area. The

pollutants were not treated for anti-seepage or coverage during the initial stage of accumulation. After several years, although the accumulated slag was treated accordingly, due to the relatively backward technology level, the soil and groundwater were severely polluted due to mining. It can reflect the overall environmental conditions of the study area. In addition, the layout of sampling points should strictly comply with the relevant requirements in the Technical Specification for Soil Monitoring (Shi et al., 2021). When collecting soil samples at each layout point, attention should be paid to multiple samples (at least three), mixed evenly, and then around 100g of soil samples should be selected and placed in clean plastic bags, and brought back to the laboratory. The soil samples brought back should be air dried in a constant temperature drying oven not exceeding 40°C, and attention should be paid to dust pollution and the entry of alkaline gases during the air drying process of the samples. Use a 10 mesh nylon sieve to remove debris such as gravel and animal residues from the air dried soil sample; Using the quartet method, select 100g of selected soil and grind it with a wooden stick or mortar; Treat with a 100 mesh nylon sieve and place it in a self sealing bag for later use.

#### (2) Soil sample treatment and determination

GB 5085.3-207 was used to carry out alkali digestion of the above collected soil samples, and GB/T 15555.4-95 was used to determine the content of heavy metal pollutants in the soil samples after alkali digestion; General analysis TAS990 atomic absorption spectrophotometer was used to determine the content of total pollutants in the soil samples; And the physicochemical properties of soil samples were determined and analyzed by conventional agricultural chemical analysis method.

#### (3) Assessment of mining area pollution soil form method

The morphological method is a screening method to achieve the purpose of diagnosis and identification by identifying the macro morphology or microstructure of tissue samples or other samples. It is a common research and diagnostic method in the fields of medicine, biology and so on. In order to realize the accurate detection of soil morphological characteristics, the morphological method is mainly used to classify the pollutants in the soil pollution samples in the mining area.

#### (4) Data analysis

All experimental data were plotted using Microsoft Office Excel 2003, Microsoft Office Visio 2003 and SigmaPlot 9.0. At the same time, SPSS software was used to analyze the experimental data, and LSD and Duncan were used to process the significant correlation test between the data, so that the significance level is  $P < 0.05$ . The overall flow of the study method is shown in Figure 3.

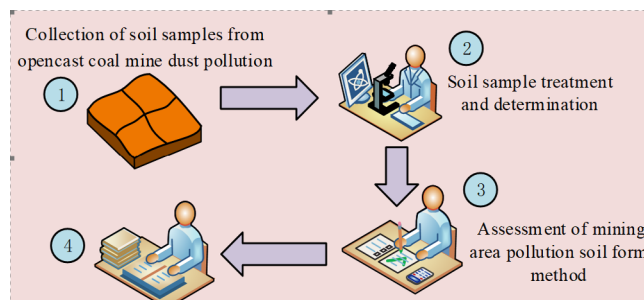


**Figure 3.** Overall flow of the study methods

#### 2.2. Analysis and Discussion of Results

Based on the above evaluation results, taking Pb and Zn contaminated soil as an example, the remediation effect of soil with P/Pb molar ratios of 0.6, 1.2, 1.8, 3.0, and 4.0 on open cut coal mine dust was analyzed under simulated room temperature conditions.

(1) Effect of different P treatment on pH and water solubility P of soil polluted by dust in open cut coal mine

The pH value of the open cut coal mines' dust-contaminated soil is significantly decreased when SSP is added to the soil samples. As the added dose level is increased, the pH value gradually decreases, with the range being between 0.5 and 1.5 units. Naturally, this is the case as acidity controls SSP in and of itself. On the contrary, if MPP is added to the dust contaminated soil samples of open cut coal mines, the soil pH value will be increased. The pH value of dust contaminated soil in open cut coal mine increases from 5.7 units to 6.3 - 6.8 units after the addition of MPP. The pH value of dust contaminated soil in open cut coal mine showed an increasing first and then decreasing trend. Among them, when the MPP dose level is 1.2, it reaches the peak, which may be caused by the competition of hydrogen phosphate for the adsorption point in the dust contaminated soil of open cut coal mine.  $\text{KH}_2\text{PO}_4$  is a strong base and weak acid salt, which usually exists in the form of  $\text{H}_2\text{PO}_4^-$  after it is added to the dust contaminated soil

samples of open cut coal mine. The ion exchange of  $\text{H}_2\text{PO}_4^-$  causes the desorption of OH ions adsorbed on the dust polluted soil of open cut coal mines, leading to an increase in soil pH value.

(2) Effect of different P treatments on water soluble Pb and Zn in soil polluted by surface coal mine dust

The concentrations of water-soluble Pb and Zn heavy metal elements in the dust contaminated soil samples of open cut coal mine after the addition of substance P have significant influences. However, due to the different varieties of substance P added, the influences are significantly different: The content of water-soluble Pb in the dust-contaminated soil of open cut coal mine treated by MPP is significantly higher than that of blank control (CK); When the phosphorus dosage level is below 1.8, the Pb content increases with the increase of phosphorus level. When it is above 1.8, the water-soluble Pb element content decreases with the increase of P level. On the contrary, the addition of SSP significantly reduced the content of Pb in the dust-contaminated soil samples of open cut coal mines, and the reduction range was 68% - 98%. Especially when SSP1.8 and SSP4.0 were used to treat the dust-contaminated soil samples of open cut coal mines, the content of water-soluble Pb in the soil was lower than the detection limit. The Zn content using SSP is less affected by the substance P contained, and the Zn content after MPP treatment changes very little, without reaching a significant difference. It can be seen that the difference in the influence of SSP and MPP on the concentration of water-soluble Pb and Zn heavy metals in soil samples contaminated by dust in open-pit mines is caused by the difference in PR. First, SSP contains abundant  $\text{Ca}^{2+}$  ions, but MPP does not. The existence of  $\text{Ca}^{2+}$  ions may promote the P-Pb precipitation reaction in the dust-polluted soil of open pit coal mine. Secondly, SSP is an acidic substance, while MPP is a neutral substance. After adding it to the dust pollution of open cut coal mines, the soil pH value in the samples will vary, and the impact of recent soil activities will also be different. The correlation analysis between the impact of dust pollution in open cut coal mines on the concentrations of water-soluble Pb, Zn, and Ca and the pH value of soil samples shows that the Zn content in the samples is negatively correlated with the soil pH value. This indicates that the activity of Zn in the dust polluted soil of open cut mines is rela-

tively low. The content of Pb and Ca in soil samples contaminated by dust from open cut mines shows a significant negative correlation, indicating that Ca in polluted soil also plays an important promoting role in the chemical reaction process of P and Pb.

(3) Effect of different P treatments on the content of Pb and Zn in the soil polluted by opencast coal mine dust

The effects of the addition of different types and dosage levels of P-containing substances on the content of exchangeable Pb and Zn in soil contaminated by opencast coal mine dust are shown in Figures 4 and 5.

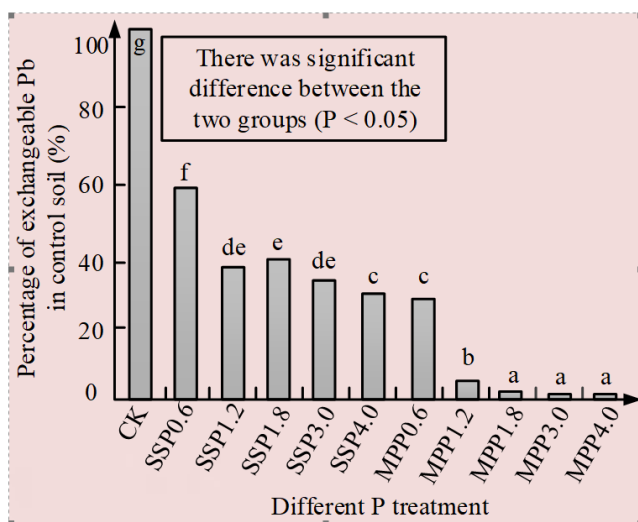


**Figure 4.** Effect of P on the content of exchangeable Pb in soil polluted by coal mine dust.

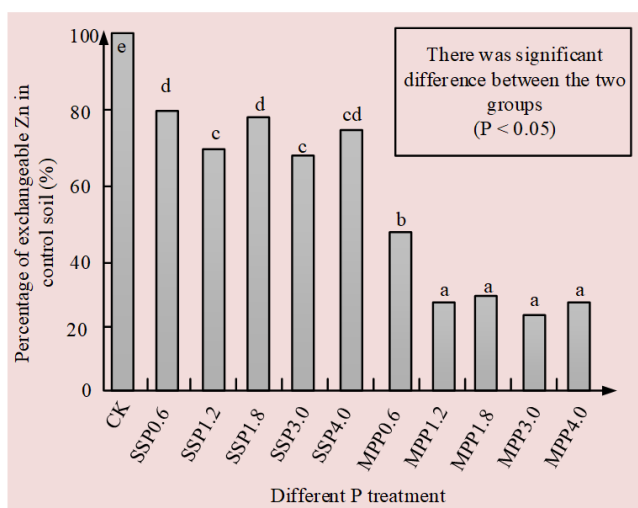


**Figure 5.** Effect of P on the content of exchangeable Zn in soil polluted by open cut coal mine dust.

This indicates that in soil samples contaminated by dust from open cut coal mines, the reduction

effect of water-soluble P composite MPP on heavy metal Pb plants is significantly higher than that of water-soluble P composite SSP. This may be related to the concentration level of water-soluble P substances containing P. The experimental results indicate that after MPP treatment, the Pb content of soil samples contaminated with heavy metals in dust sharply decreases with the increase of phosphorus levels, and the trend of change is significant. It can be divided into two regions: one region is a rapidly decreasing region, which is  $0.6 < P < 1.8$ ; The other area is a slightly decreasing area, that is, the  $P > 1.8$ . In this case, after the P level is increased, the content of exchangeable Pb heavy metals in the dust-polluted soil samples of open cut coal mines does not change significantly.

Through correlation analysis of Zn and Pb exchangeable heavy metal content in soil samples contaminated by dust from open cut mines, it was found that Pb is only negatively correlated with water-soluble P and soil pH value in the soil. However, the exchangeable heavy metal element Zn in the soil was negatively correlated with the soil pH value and water-soluble P. Previous studies have shown that the content of heavy metal elements Zn and Pb in soil contaminated by open cut coal mines dust is mainly affected by the water-soluble phosphorus content in the soil. In addition, MPP treatment is more beneficial for SSP to reduce the Pb content in the dust polluted soil of open cut mines, while the plant availability of Zn is influenced by phosphorus content and soil pH value.

### 3. Measures for control of dust pollution in open cut coal mines

#### 3.1. Prevention and Control of Dust Pollution by Engineering Units

The engineering materials such as sand, cement, and crushed stones required for open cut coal mining projects should be stockpiled in designated places. Sealing facilities such as retaining walls and coverings should be installed around the area to prevent dust from spreading widely into the air. Fine, low density, small particulate materials that are prone to dust should be stored in a completely closed warehouse or container. In addition to the construction site set up soil or cement mixer construction units, the machine must be equipped with dust at the entrance and exit dust-proof devices. When there is a grade-4 or above wind in a construc-

tion city, it is necessary to prohibit the construction of all large open cut coal mines projects and the relevant earthwork construction on the foundation, the transportation of construction garbage and the transportation of relevant dregs. The Construction waste generated in the construction of the open pit coal mine can be treated and transported by taking corresponding dust spraying and pressure measures. The excavation, support, and transportation time of the foundation soil during the construction process of open cut coal mines should also be strictly controlled. When transporting vehicles to load and unload construction garbage, it is strictly prohibited to throw construction garbage directly into the air and unload them randomly so as to eliminate the pollution caused by secondary fugitive dust.

### 3.2. Control of Dust Pollution in Open Cut Coal Mines

Based on the people's enthusiasm for living environment and human health, the typical dust pollution events in open cut coal mines are discussed openly and universally. Especially after large-scale open cut coal mine pollution incidents or medical and health incidents occur, reasonable public opinion guidance can be used to raise public awareness of dust pollution in open cut coal mines. This can attract more attention, promote the formation of a sense of crisis among the public, and spontaneously supervise urban construction activities. In addition, the relevant streets, neighborhood committees can organize people-oriented supervision team, directly involved in the construction of open cut coal mines supervision. Relevant departments can set up air monitoring points in densely populated areas of urban construction projects. This method enables the supervision team and the public to clearly and in real-time observe the concentration data of pollution dust generated during the construction process of open-pit coal mines. This intuitive data expression can make the public more aware of the seriousness of the dust pollution during the construction of opencast coal mines and can have direct contact with the activity of air concentration than the medical health report and the numbers described by reporters and relevant experts in the public media. In addition, for some long-term environmental protection volunteer teams, it is necessary to change the mode of urban environmental protection activities. In addition to the environmental protection department's own fixed environmental protection

volunteers, the majority of the public are random, short-term one-time participation. This kind of participation cannot meet the requirement of popularization of dust pollution knowledge and continuous improvement of environmental protection.

### 3.3. Improving Government Governance Initiatives

Clarifying the overall positioning standards is the basis for taking measures to protect the atmospheric environment and control the dust pollution of surface coal mines. Relevant environmental protection departments need to improve the positioning standards for dust pollution of surface coal mines. The relevant governance departments should take into account the protection of public health and the protection of the atmospheric environment, and formulate and clarify standards for atmospheric dust pollution during the construction of open cut coal mines. In addition, government departments need to rationally use economic means to change surface coal mine dust pollution control into government behavior. The concept of urbanization has led to the continuous increase of new construction projects in modern cities and serious dust in the open cut coal mine construction.

## 4. Conclusions and recommendations

Based on the above analysis and tests, the following conclusions have been drawn:

(1) Adding SSP to the soil samples polluted by coal mine dust in the open cut obviously reduced the pH of the soil; Adding MPP increased the pH of the soil, which was related to the acidity and alkalinity of the soil added with substance containing P.

(2) With the addition of phosphorus containing substances, the water-soluble phosphorus content in the dust polluted soil of open cut coal mines significantly increases, but the impact of different varieties on their phosphorus content is different, with MPP>SSP.

(3) The decrease in Zn content in soil samples contaminated by dust from open-pit coal mines is similar to that of Pb, with MPP>SSP, but different from Pb.

(4) Both SSP and MPP can significantly reduce the heavy metal content of Pb and Zn in the soil polluted by open coal mine dust, and the order of decreasing is MPP > SSP.

(5) The exchangeable heavy metal element Pb was only negatively correlated with water soluble

P in soil; While the exchangeable heavy metal element Zn was negatively correlated with both soil pH and water soluble P, but was mainly controlled by soil pH.

Although this study can effectively analyze the dust pollution characteristics of open cut coal mines, only the LSD method and Duncan method were used to test the significance of the data during the experimental process. To ensure the effectiveness of the dust pollution control methods proposed in the study, more methods need to be used to validate them, including practical applications, in order to improve the effectiveness of testing.

From the point of view of monitoring, evaluation and control, there are a lot of research work to be done in depth, such as: Improving the real-time monitoring system and early warning system for open cut dust; Studying the calculation model of

## References

- Benitez-Polo, Z. and Velasco, L.A. 2020. Effects of suspended mineral coal dust on the energetic physiology of the Caribbean scallop *Argopecten nucleus* (Born, 1778). *Environment Pollution*, 260(5): 114000.
- Coglianesi, J., Gerarden, T.D. and Stock, J.H. 2020. The effects of fuel prices, environmental regulations, and other factors on U.S. coal production, 2008-2016. *The Energy Journal*, 41(1): 55-81.
- Ding, X., Xu, G., Liu, W.V., 2019. Effect of polymer stabilizers' viscosity on red sand structure strength and dust pollution resistance. *Powder Technology*, 352(4): 117-125.
- Finke, R.G., Watzky, M.A. and Whitehead, C.B. 2020. Response to "particle size is a primary determinant for sigmoidal kinetics of nanoparticle formation: A "disproof" of the Finke-Watzky (F-W) nanoparticle nucleation and growth mechanism". *Chemistry Materials*, 32(8): 3657-3672.
- Guo, S.L., Yan, Z., Yuan, S.J., 2021. Inhibitory effect and mechanism of L-ascorbic acid combined with tea polyphenols on coal spontaneous combustion. *Energy*, 229(11): 120651.
- dust concentration in open cut mines; Studying the influence of dust on the production cost of mines, revealing the harm of dust pollution, and improving the subjective initiative of mine enterprises in controlling dust; Studying the measures for reducing, suppressing and removing dust in open cut mines, etc. The further in-depth research will help promote the development of green mining technology, reduce the impact of coal mining on the environment, improve the society's awareness of coal damage to the environment, and contribute to the healthy development of the coal industry.

## Funding

The research is supported by the general project of National Natural Science Foundation of China "integrated technology of ecological environment restoration and mining in open pit coal mine based on green degree". Project Number: (No. 51474119).

Heidari, M., Darijani, T. and Alipour, V. 2021. Heavy metal pollution of road dust in a city and its highly polluted suburb; quantitative source apportionment and source-specific ecological and health risk assessment. *Chemosphere*, 273(7): 129656.

Jing, D.J., Jia, X., Ge, S.C., 2021. Numerical simulation and experimental study of vortex blowing suction dust control in a coal yard with multiple dust production points. *Powder Technology*, 288(8): 554-565.

Jiskani, I. M., Cai, Q. X., Wei, Z., 2021. Green and climate-smart mining: A framework to analyze open-pit mines for cleaner mineral production. *Resources Policy*, 71(1):102007-102019.

Jiskani, I. M., Cai, Q., Zhou, W., 2022. An integrated fuzzy decision support system for analyzing challenges and pathways to promote green and climate smart mining. *Expert Systems with Applications*, 2022, 188(2):116062

Luo, H., Zhou, W., Jiskani, I. M., et al, 2021. Analyzing Characteristics of Particulate Matter Pollution in Open-Pit Coal Mines: Implications for Green Mining. *Energies*, 2021, 14(9):2680.

Kazi, T.G., Lashari, A.A., Ali, J., 2019. Volatilization of toxic elements from coal samples of Thar coal field, after burning at different temperature and their mobility from ash: Risk assessment. *Chemosphere*, 217(2): 35-41.

- Ma, Q., Nie, W., Yang, S., et al., 2020. Effect of spraying on coal dust diffusion in a coal mine based on a numerical simulation. *Environment Pollution*, 264(2): 114717.
- Markovi, J., Mievi, S., Delali, M. et al., 2021. Minimum ignition energy of lignite and brown coal dust clouds in coal with and without interlayers. *Quarterly Journal of Engineering Geology and Hydrogeology*, 9(2021): 98-106.
- Meha, D., Pfeifer, A., Dui, N., et al., 2020. Increasing the integration of variable renewable energy in coal-based energy system using power to heat technologies: The case of Kosovo. *Energy*. 212(2), 118762.
- Shi, J., Huang, W., Han, H. et al., 2021. Pollution control of wastewater from the coal chemical industry in China: Environmental management policy and technical standards. *Renewable and Sustainable Energy Reviews*, 143(4): 110883.
- Tong, L., Chen, X., Zhang, Y., et al., 2019. Adhesion and desorption characteristics of high-temperature condensed flue gas dust on filter material surface. *Powder Technology*, 354(9): 760-764.
- Trechera, P., Moreno, T., Córdoba, P., et al., 2021. Comprehensive evaluation of potential coal mine dust emissions in an open-pit coal mine in Northwest China. *International Journal of Coal Geology*, 235(15): 103677.
- Wirth, V., Bubel, P., Eichhorn, J., et al., 2020. The role of wind speed and wind shear for banner cloud formation. *Journal of the Atmospheric Sciences*, 77(4): 125-136.
- Wang, Z., Zhou, W., Jiskani, I. M., et al, 2022. Annual dust pollution characteristics and its prevention and control for environmental protection in surface mines. *Science of The Total Environment*, 2022, 825(15):153949





## Evaluating machine utilization times for roadheaders used in coal mines: Multiple regression and artificial neural network analyses

Sair Kahraman<sup>a,\*</sup>, Masoud Rostami<sup>b,\*\*</sup>, Behnaz Dibavar<sup>b,\*\*\*</sup>

<sup>a</sup>Hacettepe University, Mining Engineering Department, Ankara, TÜRKİYE

<sup>b</sup>Hacettepe University, Graduate School of Science and Engineering, Ankara, TÜRKİYE

Received: 7 June 2023 \* Accepted: 17 October 2023

### ABSTRACT

Roadheaders are extensively utilized for tunnel heading rock engineering applications all over the world. To create a work plan and calculate costs, it is critical to forecast roadheader performance as precisely as possible. Machine utilization time (MUT) is required for the calculation of daily advance rate of roadheaders. This paper investigates the values of MUT for roadheaders used in underground coal mines. The performance measurements were conducted on fifty different locations for axial machines and thirty-nine different locations for transverse machines. MUT values vary from 15 % to 37.5 % with an average of 26.3 % for axial roadheaders, and vary from 6.9 % to 37.9 % with an average of 18.4 % for transvers roadheaders. The average MUT is 25.4% for all measurements. The percentage of average support time approximately equals to the average MUT. Multiple regression and artificial neural network models were also developed for estimating MUT. Concluding remark is that the determined MUT values and the derived estimation models for roadheaders will be very useful for coal miners.

**Keywords:** Coal mining, Roadheader, Machine utilization time

### Introduction

In rock engineering projects, rocks are excavated by drilling and blasting method or by mechanized excavation method. Mechanical cutting of rocks and coals has been increasing day by day in developed and developing countries. Roadheaders are commonly used in mining for gallery drivages and in civil engineering for tunnel excavations. It is essential to predict roadheader performance as accurately as possible for making a work schedule and estimating costs.

Different investigators have proposed several performance prediction equations for roadheaders (Gehring, 1989; Bilgin et al., 1990; Rostami et al., 1994; Copur et al., 1998; Thuro and Plinnin-

ger, 1999; Göktan and Güneş, 2005; Tumac et al., 2007; Ocağ and Bilgin, 2010; Ebrahimabadi et al., 2011; Abdolreza and Yakhchali, 2013; Kahraman and Kahraman, 2016; Kahraman et al., 2019). Using these models, net cutting rate (NCR) is calculated. However, machine utilization time (MUT) is required for the calculation of daily advance rate (ARd) of roadheaders as shown in the following equations:

$$AR_d = V/A \quad (1)$$

$$V = NCR.MUT.WT_d \quad (2)$$

where, ARd, is daily advance rate (m/day), V is daily excavated volume (m<sup>3</sup>/day), A is cross-section area of tunnel (m<sup>2</sup>), NCR, net cutting rate (m<sup>3</sup>/h), MUT is machine utilization time (%), and WTd is daily working time (h/day).

\*Corresponding author: s.kahraman@hacettepe.edu.tr • <https://orcid.org/0000-0001-7903-143X>

\*\* rustami.masud@gmail.com • <https://orcid.org/0000-0001-5411-6939>

\*\*\* bdibavar@gmail.com • <https://orcid.org/0000-0002-2680-4192>

<https://doi.org/10.30797/madencilik.1310876>

MUT is the percentage of time used only for excavation during the entire shift or day. Several operational and organizational variables affect MUT. The remaining time from MUT consists of pauses such as support installation, muck haulage, breakdown, and maintenance. The correct selection of MUT is at least as important as the NCR estimation. Even if NCR is estimated correctly, if the MUT is selected incorrectly, the average advance rate and project duration will be incorrectly estimated. Therefore, often unrecoverable problems and large financial losses occur.

There is no detailed study in the literature on the MUT values of roadheaders. McFeat-Smith and Fowell (1979) evaluated roadheader performances in sandstone, mudstone and siltstone formations and observed that the MUT values ranged between 40 % and 60 %. Copur et al. (2001) stated that MUT ranged between 25 % and 50 %. MUT was measured as 47 % for the Küçüküsu sewage tunnel (Bilgin et al., 2005) and as 28.2 % for the Kadıköy-Kartal metro tunnel (Ocak, 2008). It is quite remarkable that the MUT in Hereke tunnel, which is 38 % in straight excavations, decreases to 8 % in uphill excavations (Bilgin et al., 2004). Bilgin et al. (2014) explain that MUT varies from 20 % and 35 % for the tunnel excavation requiring steel supports, and varies from 30 % and 50 % for the tunnel excavation requiring rock bolts, shotcrete, and wire mesh.

According to literature data, MUT can vary in a wide range, from 8 % to 60 %. It is quite difficult to decide which value should be used in coal mining. This study investigates the range of MUT values for roadheaders used in coal mines. For this purpose, the performance measurements of roadheaders were conducted in seven different underground coal mines in Türkiye and the results were evaluated to determine the MUT values.

### 1. Materials and methods

Underground coal mines located in different areas of Türkiye were visited for the field studies. Axial and transvers type roadheaders were observed during the excavation of roadways and comprehensive perfor-

mance data for were collected for the analyses.

The overall performances of roadheaders for each coal mine was first evaluated using pie charts and MUT values were calculated for each case. Then, the data was evaluated using multiple regression and artificial neural network analyses. Multiple regression and artificial neural network models were also derived for the estimation of MUT values.

### 2. Performance measurements

Axial and transvers type roadheaders' performances were measured in seven different lignite collieries in Türkiye. The study covers one enterprise from Amasra and Dodurga region, two enterprises from Çayırhan region and three enterprises from the Soma region.

During the performance measurements, excavation time, support time, mucking time, maintenance time, machine breakdown time, electric break-down time, shift change time, other waiting time were recorded. The experience of operators, the age of machines, the experience of companies, the inclination of roadways, the cross-sectional areas of roadways were also noted.

Performance measurements were made in as many different conditions as possible. The measurements were carried out in fifty different locations for axial machines and thirty-nine different locations for tranverse machines.

### 3. Results and discussions

The summaries of the MUT values and the parameters affecting MUT are given in Table 1 and 2 for axial and transvers roadheaders, respectively. MUT values range from 15 % to 37.5 % with an average of 26.3% for axial roadheaders. For transvers roadheaders, MUT values vary from 6.9 % to 37.9 % with an average of 18.4 %. The values have wide ranges for the experience of operators, the age of machines, the experience of companies, the inclination of roadways, the cross-sectional area of roadways.

**Table 1.** *The parameters affecting MUT for axial roadheaders.*

Statistical parameter	Excavation time (MUT) (%)	Operator experience (years)	Machine age (years)	Company experience (years)	Roadway inclination (o)	Roadway cross-sectional area (m <sup>2</sup> )
Number of observ.	50	50	50	50	50	50
Minimum	15.0	0.5	1.0	2.0	- 18.0	12.0
Maximum	37.5	23.0	32.0	20.0	+ 4.0	23.5
Average	26.3	8.3	18.0	13.4	-3.70	20.6
Standard deviation	± 6.2	± 8.1	± 13.8	± 8.0	± 7.9	± 3.9

**Table 2.** *The parameters affecting MUT for transvers roadheaders.*

Statistical parameter	Excavation time (MUT) (%)	Operator experience (years)	Machine age (years)	Company experience (years)	Roadway inclination (o)	Roadway cross-sectional area (m <sup>2</sup> )
Number of observ.	39	39	39	39	39	39
Minimum	6.9	2.0	5.0	1.0	- 12.0	14.0
Maximum	37.9	15.0	39.0	15.0	+ 15.0	28.0
Average	18.4	5.6	23.2	9.0	1.6	20.0
Standard deviation	± 8.3	± 3.9	± 16.5	± 6.3	± 7.8	± 4.5

The summaries of the MUT values, the percentages of stoppages, and other job times are given in Table 3-9 for each company, respectively. The overall performances of roadheaders for each coal mine were plotted as shown in Fig. 1.

The MUT values vary from 17.7% to 56.2% with an average of 31.8% for coal mine A. Support work takes the most time (27.1%) after the MUT value. Since there is no electric break down during the performance measurements, the time for electric break down is zero.

For coal mine B, the average MUT value is 23.5%, with values ranging from 9.8% to 31.9%. Other waiting time is very high (35.8%) due to the breakdown of the main belt conveyor of the mine. Machine break downtime has the lowest value with 1.2%.

With an average of 26.0% for coal mine C, the MUT values range from 20.3% to 32.5%. The percentage of support time (29%) is higher than that of the MUT value. The mucking time is also relatively high (%17). The lowest waiting percentage is 2.9% for electric break downtime.

The average MUT value for coal mine D is 17.2%, with values ranging from 6.9% to 33.3%. Support time is too high (42.9%) due to the fact that mine operates in harsh conditions such as high depth, excessive water flow, and highly fractured formations. Electric break-

down time has the lowest percentage, 2.0%.

The MUT values vary from 2.3.7% to 37.9% with an average of 22.6% for coal mine E. The percentage of support time (22.8%) is the same as the MUT value. Electric breakdown time is also high (%15.1). Machine break downtime has the lowest value with 4.6%.

For coal mine F, the average MUT value is 31.2%, with values ranging from 15.6% to 41.6%. The percentage of support time (32.0%) is approximately the same as the MUT value.

The percentages of waiting times are zero for mucking time, maintenance time, machine break-down time, electric break-down time. However, this performance data only belongs to three measurements.

The average MUT value for coal mine G is 24.6%, with values ranging from 9.3% to 35.4%. Other waiting time is relatively high (21.2%) due to the breakdown of the main shaft haulage system of the mine. Maintenance time has the lowest value with 4.1%. However, this performance data consists of only three measurements.

The overall performances of roadheaders for all coal mines are listed in Table 10 and is plotted in Fig. 1h. The average MUT is 25.4%. The percentage of average support time (23.5%) is roughly equal to the average MUT. The percentage times of ucking, shift change, and other stoppages significantly affect the MUT value.

**Table 3.** *The summarized data for the MUT of roadheaders used in coal mine A.*

Statistical parameter	Excavation time (MUT) (%)	Support time (%)	Mucking time (%)	Maintenance time (%)	Machine break-down time (%)	Electric break-down time (%)	Shift change time (%)	Other waiting time (%)
Number of observ.	12	12	12	12	12	12	12	12
Minimum	17.7	12.5	0.0	6.2	0.0	0.0	12.5	0.0
Maximum	56.2	39.6	29.2	13.6	10.4	0.0	16.7	43.8
Average	31.8	27.1	11.9	8.4	1.0	0.0	12.8	6.9
Standard deviation	± 11.7	± 8.4	± 11.7	± 3.3	± 6.3	± 0.0	± 1.2	± 12.8

**Table 4.** *The summarized data for the MUT of roadheaders used in coal mine B.*

Statistical parameter	Excavation time (MUT) (%)	Support time (%)	Mucking time (%)	Maintenance time (%)	Machine break-down time (%)	Electric break-down time (%)	Shift change time (%)	Other waiting time (%)
Number of observ.	7	7	7	7	7	7	7	7
Minimum	9.8	3.1	0.0	0.0	0.0	0.0	6.3	0.0
Maximum	31.9	37.5	25.0	9.4	8.1	12.5	12.5	77.7
Average	23.5	17.5	7.8	4.0	1.2	3.0	7.2	35.8
Standard deviation	± 7.4	± 14.0	± 8.7	± 3.9	± 3.1	± 4.8	± 2.4	± 23.5

**Table 5.** *The summarized data for the MUT of roadheaders used in coal mine C.*

Statistical parameter	Excavation time (MUT) (%)	Support time (%)	Mucking time (%)	Maintenance time (%)	Machine break-down time (%)	Electric break-down time (%)	Shift change time (%)	Other waiting time (%)
Number of observ.	17	17	17	17	17	17	17	17
Minimum	20.3	20.8	11.3	6.3	0.0	0.0	12.5	0.0
Maximum	32.5	38.2	24.0	6.5	8.3	6.3	12.5	9.3
Average	26.0	29.0	17.0	6.3	3.7	2.9	12.5	2.7
Standard deviation	± 3.4	± 6.8	± 4.6	± 0.1	± 2.9	± 3.2	± 0.0	± 3.4

**Table 6.** *The summarized data for the MUT of roadheaders used in coal mine D.*

Statistical parameter	Excavation time (MUT) (%)	Support time (%)	Mucking time (%)	Maintenance time (%)	Machine break-down time (%)	Electric break-down time (%)	Shift change time (%)	Other waiting time (%)
Number of observ.	25	25	25	25	25	25	25	25
Minimum	6.9	8.5	0.0	0.0	0.0	0.0	6.3	0.0
Maximum	33.3	76.3	53.8	15.6	31.3	14.6	12.5	27.5
Average	17.2	42.9	12.7	4.6	4.1	2.0	6.8	9.8
Standard deviation	± 7.0	± 20.9	± 11.9	± 5.3	± 9.1	± 4.1	± 1.7	± 9.0

**Table 7.** *The summarized data for the MUT of roadheaders used in coal mine E.*

Statistical parameter	Excavation time (MUT) (%)	Support time (%)	Mucking time (%)	Maintenance time (%)	Machine break-down time (%)	Electric break-down time (%)	Shift change time (%)	Other waiting time (%)
Number of observ.	31	31	31	31	31	31	31	31
Minimum	2.3	0.0	0.0	0.0	0.0	0.0	2.1	0.0
Maximum	37.9	59.4	81.0	39.6	18.8	73.8	9.4	75.0
Average	22.6	22.8	14.0	4.8	4.6	15.1	5.8	10.3
Standard deviation	± 10.9	± 13.4	± 17.0	± 7.2	± 6.8	± 17.0	± 1.5	± 14.7

**Table 8.** *The summarized data for the MUT of roadheaders used in coal mine F.*

Statistical parameter	Excavation time (MUT) (%)	Support time (%)	Mucking time (%)	Maintenance time (%)	Machine break-down time (%)	Electric break-down time (%)	Shift change time (%)	Other waiting time (%)
Number of observ.	3	3	3	3	3	3	3	3
Minimum	15.6	9.4	0.0	0.0	0.0	0.0	17.7	0.0
Maximum	41.6	45.8	0.0	0.0	0.0	0.0	17.7	57.3
Average	31.2	32.0	0.0	0.0	0.0	0.0	17.7	19.1
Standard deviation	± 13.8	± 19.7	± 0.0	± 0.0	± 0.0	± 0.0	± 0.0	± 33.1

**Table 9.** *The summarized data for the MUT of roadheaders used in coal mine G.*

Statistical parameter	Excavation time (MUT) (%)	Support time (%)	Mucking time (%)	Maintenance time (%)	Machine break-down time (%)	Electric break-down time (%)	Shift change time (%)	Other waiting time (%)
Number of observ.	3	3	3	3	3	3	3	3
Minimum	9.3	24.0	12.5	0.0	0.0	0.0	12.5	13.6
Maximum	35.4	26.0	12.5	6.2	0.0	0.0	12.5	35.5
Average	24.6	25.0	12.5	4.1	0.0	0.0	12.5	21.2
Standard deviation	± 13.6	± 1.0	± 0.0	± 3.6	± 0.0	± 0.0	± 0.0	12.4

**Table 10.** *The summarized data for the MUT of roadheaders used in all coal mines.*

Coal mine	Average excavation time (MUT) (%)	Support time (%)	Mucking time (%)	Maintenance time (%)	Machine break-down time (%)	Electric break-down time (%)	Shift change time (%)	Other waiting time (%)
A	31.8	27.1	11.9	8.4	1.0	0.0	12.8	6.9
B	23.5	17.5	7.8	4.0	1.2	3.0	7.2	35.8
C	26.0	29.0	17.0	6.3	3.7	2.9	12.5	2.7
D	17.2	42.9	12.7	4.6	4.1	2.0	6.8	9.8
E	22.6	22.8	14.0	4.8	4.6	15.1	5.8	10.3
F	31.2	32.0	0.0	0.0	0.0	0.0	17.7	19.1
G	24.6	25.0	12.5	4.1	0.0	0.0	12.5	21.2
Average	25.3	23.5	10.8	4.6	2.1	5.8	10.9	12.4

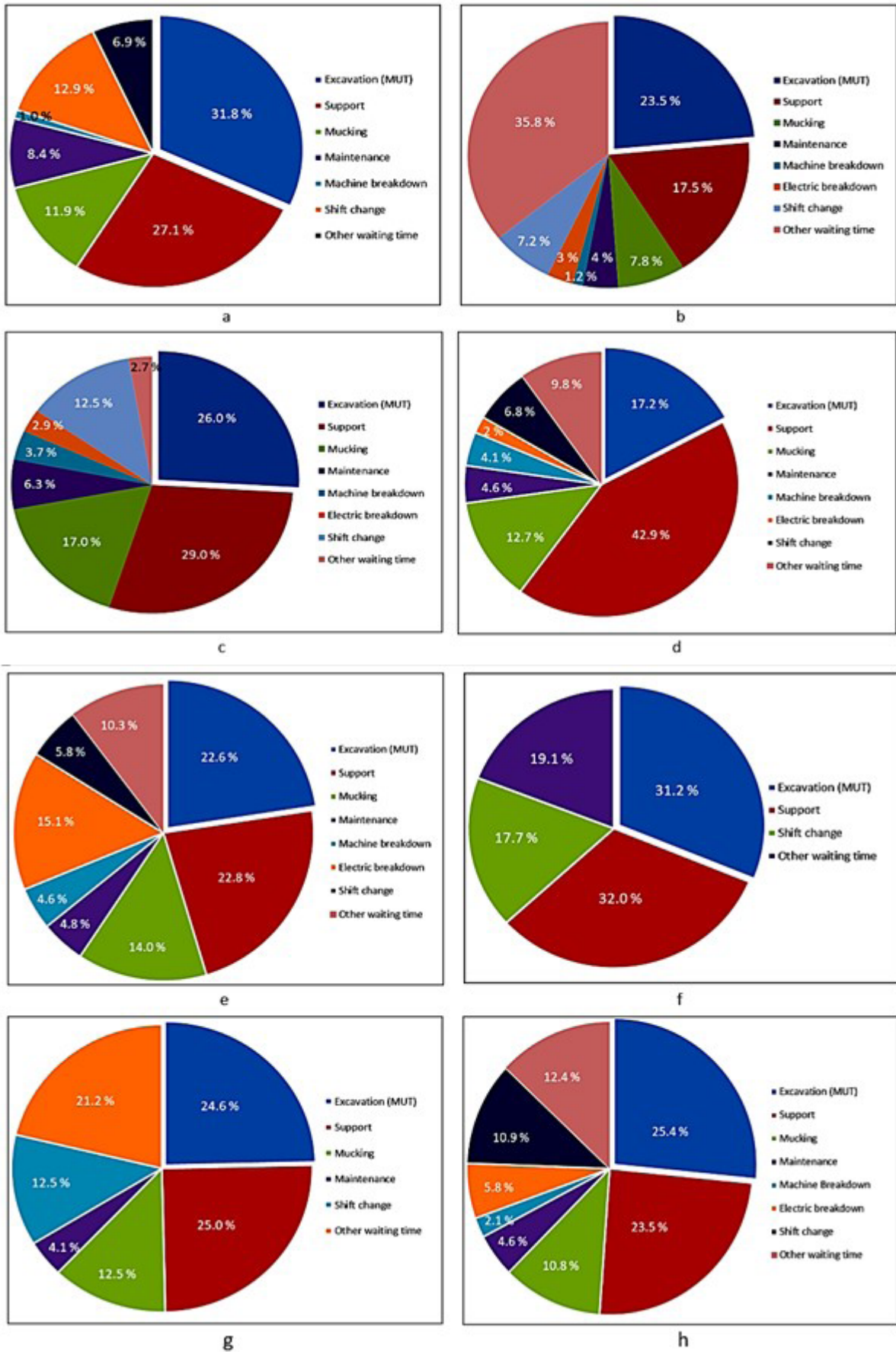


**Figure 1.** The overall performances of roadheaders for coal mine A (a), coal mine B (b), coal mine C (c), coal mine D (d), coal mine E (e), coal mine F (f), coal mine G (g), and all coal mines (h).

### 3.1. Multiple regression analysis

The results were also evaluated for the development of the estimation models for MUT. MUT is influenced by a variety of factors; hence it cannot be studied using simple regression models. The analysis must therefore be performed using multiple regression techniques. The experience of operators, the age of machines, the experience of companies, the inclination of roadways, and the cross-sectional area of roadways were all added to the multiple regression analysis as independent variables. The derived equations and the correlation coefficients ( $r$ ) are as follows:

$$\begin{aligned} \text{MUT}_a &= -0.21E_o - 0.31A_m + 0.80E_c + 0.40\alpha - 0.85A + 41.92 \\ r &= 0.78 \end{aligned} \quad (3)$$

$$\begin{aligned} \text{MUT}_t &= 0.26E_o - 0.12A_m + 1.95E_c - 0.43\alpha + 2.38A - 44.61 \\ r &= 0.76 \end{aligned} \quad (4)$$

where  $\text{MUT}_a$  is the machine utilization of axial roadheaders (%),  $\text{MUT}_t$  is the machine utilization of transvers roadheaders (%),  $E_o$  is the experience of operator (years),  $A_m$  is the age of machine (years),  $E_c$  is the experience of company (years),  $\alpha$  is the inclination of roadway ( $^\circ$ ),  $A$  is the cross-sectional area of roadway ( $\text{m}^2$ ).

It can be said that the correlation coefficients of Eqs. (3 and 4) is strong. The scatter graphs of measured and predicted MUT values were also plotted for checking the prediction capability of the derived equations. The data points should ideally be scattered around 1:1 diagonal straight line on the plot of measured versus predicted value. A systematic deviation from this line may show that larger errors tend to accompany larger predictions, suggesting non-linearity in one or more variables. As illustrated in Figs. 2 and 3, the data points are scattered almost evenly around the 1:1 line. Therefore, it can be said that the models are valid. It can be said that the equations can be used reliably for the estimation of MUT values of roadheaders.

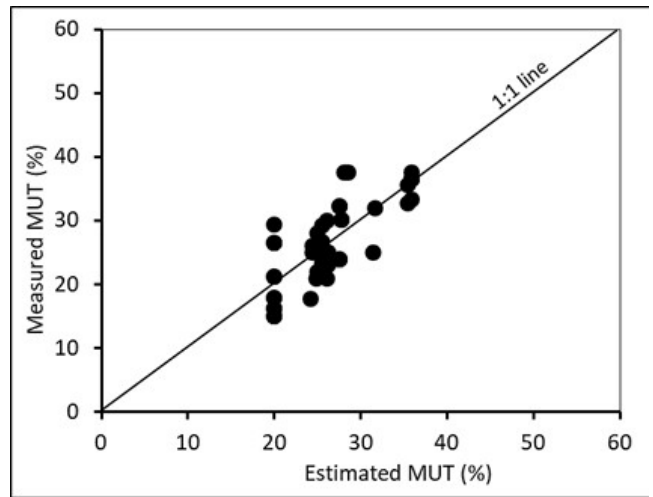


**Figure 2.** Predicted versus measured MUT for Eq. (3).

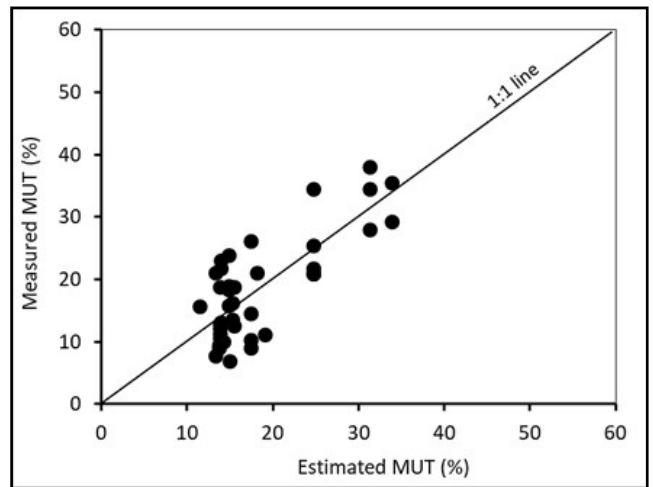


**Figure 3.** Predicted versus measured MUT for Eq. (4).

### 3.2. Artificial neural network analysis

Artificial neural network (ANN) analyses were also performed in MATLAB environment for the expectation of more reliable models than the multiple regression models. ANNs are incredibly simplified representations of the neural systems seen in the human brain. These models are made up of a networked assemblage of neurons, which are basic processing units, arranged in layers. Every neuron in one layer is linked to the neurons in the next layer, and so on. In this research, a Multi Layered Perception neural network was utilized (MLP).

For axial type roadheaders, a total of 50 data were used. The first data set, which had 34 data, was utilized to train the network for Model I. For the validation and testing of Model I, 8 data sets were utilized, respectively. For transverse type roadheaders, a total of 39 data were used. The network was trained using the first data set, whi-

ch had 25 data. Model II was validated and tested using 7 data sets, respectively. While constructing the models, trial-and-error procedure was used to find good models. Table 11 displays the structures and algorithm used throughout the training phase. The training progresses were also given in Table 12 and 13.

**Table 11.** *The structures of the ANN models for the prediction of differential stress.*

Model no	Number of input neurons	Number of hidden neurons	Number of output neurons	Network type	Transfer function	Training algorithm
I	5	6	1	Feed-forward back propagation	Tanjant sigmoid	Levenberg-Marquardt backpropagation algorithm (trainlm)
II	5	5	1	Feed-forward back propagation	Tanjant sigmoid	Levenberg-Marquardt backpropagation algorithm (trainlm)

**Table 12.** *The training progress for Model I.*

Unit	Initial Value	Stopped value	Target Value
Epoch	0	11	1000
Elapsed Time	-	00:00:00	-
Performance	169	9.99	0
Gradient	269	7.03e-08	1e-07
Mu	0.001	1e-05	1e+10
Validation Checks	0	6	6

**Table 13.** *The training progress for Model II.*

Unit	Initial Value	Stopped value	Target Value
Epoch	0	32	1000
Elapsed Time	-	00:00:00	-
Performance	224	20.9	0
Gradient	649	20.4	1e-07
Mu	0.001	0.1	1e+10
Validation Checks	0	6	6

The scatter diagrams of observed and estimated values can be presented in order to examine the estimating capabilities of the developed models. On a plot of estimated vs observed data, the points

should ideally be dispersed over the 1:1 diagonal straight line. A point that lies on the line denotes a precise estimate. A systematic deviation from this line may reveal, for instance, that higher errors go along with larger estimations, which suggests that one or more variables are not linear. The plots for predicted vs. measured MUT are indicated in Figs. 4 and 5, respectively for the Model I, and II. The fact that the points are distributed consistently around the diagonal line in the graphs suggests that the models are valid.

The values of mean square error (MSE) and correlation coefficient (r) are listed in Table 14 for the ANN models. MSE values are low and r values are generally too high. Therefore, it can be said that ANN models are reasonable. In comparison to multiple regression models, ANN models' r values are noticeably greater.

**Table 14.** *MSE and r values for the developed ANN models.*

	Model I		Model II	
	MSE	r	MSE	r
Training	10.83	0.83	23.72	0.81
Validation	6.01	0.97	13.26	0.93
Test	8.99	0.93	16.06	0.90

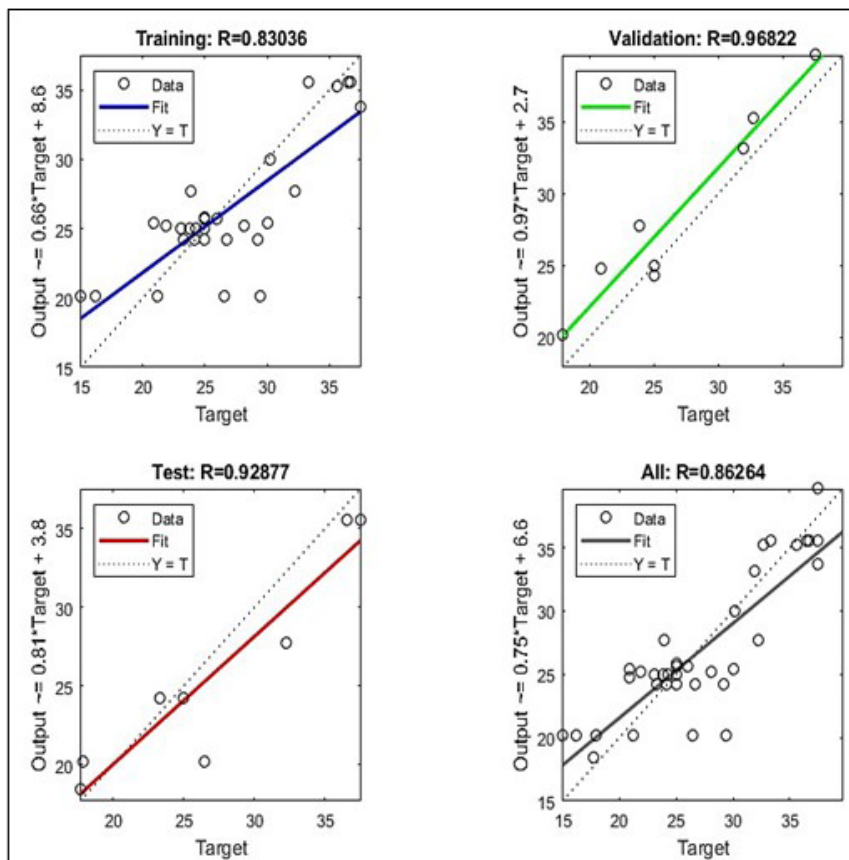


**Figure 4.** Predicted vs. measured MUT values for ANN Model I.

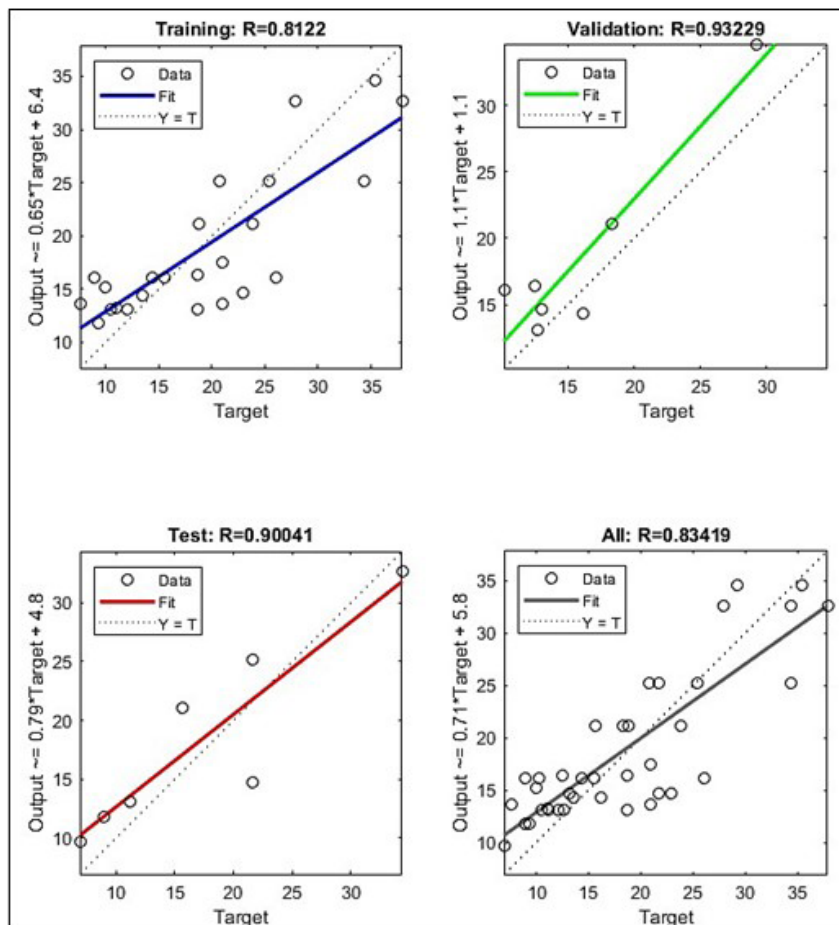


**Figure 5.** Predicted vs. measured MUT values for ANN Model II.

#### 4. Conclusions

The MUT values of roadheaders used in underground coal mines were assessed. The study's findings can be summarized as follows:

The average MUT value is 26.3% for axial roadheaders, and 18.4% for transvers roadheaders.

The average MUT is 25.4% for both type of machines and all measurements.

The average support time percentage is approximately equal to the average MUT.

#### Acknowledgement

The authors thank TUBITAK (The Scientific and Technological Research Council of Turkey) for the support of the project (Project No. 217M740). The authors also thank Park Termik Elektrik Sanayi ve

The derived multiple regression equations can be used for estimating MUT values

Since the correlation coefficients of the ANN models are quite high compared to the multiple regression models, these models can be preferred for more reliable estimation.

It can be concluded that the determined MUT values and the developed estimation models for roadheaders will be very helpful for coal miners.

Ticaret A.Ş., Hattat Enerji ve Maden Ticaret A.Ş., Polyak Eynez Enerji Üretim Madencilik San. ve Tic. A.Ş., İmbat Madencilik Enerji Turizm San. Tic..A.Ş., Demir Export A.Ş., YS Madencilik San. ve Tic. Ltd. Ş. and Kömür İşletmeleri A.Ş. for allowing the field studies.

#### References

- Abdolreza, Y.C., Yakhchali, S.H.. 2013. A new model to predict roadheader performance using rock mass properties. *Journal of Coal Science and Engineering*. 19 (1), 51-56.
- Bilgin, N., Seyrek, T., Erdinc, E., Shahriar, K. 1990. Roadheaders clean valuable tips for Istanbul Metro. *Tunnels and Tunnelling*. 22, 29-32.
- Bilgin, N., Dincer, T., Copur, H., Erdogan, M. 2004. Some geological and geotechnical factors affecting the performance of a roadheader in an inclined tunnel. *Tunnelling and Underground Space Technology*. 19, 629-636.
- Bilgin, N., Tumac, D. Feridunoglu, C., Karakas, A.R., Akgul, M. 2005. The performance of a roadheader in high strength rock formations in Küçüküsu tunnel. *Proc. of the 31th ITA-AITES World Tunnel Congress*. Istanbul, Turkey, pp. 815-820.
- Bilgin, N., Copur, H., Balci, C. 2014. *Mechanical Excavation in Mining and Civil Industries*. CRC Press, Taylor and Francis Group.
- Copur, H., Ozdemir, L., Rostami, J. 1998. Roadheader Applications in Mining and Tunneling Industries. Annual Meeting of American Society for Mining, Metallurgy and Exploration (SME). Orlando, Florida, March 10-12, Preprint Number: 98-185.
- Copur, H., Tuncdemir, H., Bilgin, N., Dincer, T. 2001. Specific energy as a criterion for the use of rapid excavation systems in Turkish mines. *The Institution of Mining and Metallurgy, Transactions Section-A Mining Technology*. 110, A149-A157.
- Ebrahimabadi, A., Goshtasbi, K., Shahriar, K., CheraghiSeifabad, M. 2011. A model to predict the performance of roadheaders based on rock mass brittleness index. *Journal of the Southern African Institute of Mining and Metallurgy*. 111, 355-364.
- Gehring, K.H., 1989. A cutting comparison. *Tunnels and Tunnelling*. 21, 27-30.
- Göktaş, R.M., Güneş, N. 2005. A comparative study of Schmidt hammer testing procedures with reference to rock cutting machine performance prediction. *International Journal of Rock Mechanics & Mining Sciences*. 42(3), 466-472.
- Kahraman, E., Kahraman, S. 2016. The performance prediction of roadheaders from easy testing methods. *Bulletin of Engineering Geology and the Environment*. 75, 1585-1596.
- Kahraman, S., Aloglu, A. S., Aydın B., Saygın, E. 2019. The needle penetration index to estimate the performance of an axial type roadheader used in a coal mine. *Geomechanics and Geophysics for Geo-Energy and Geo-Resources*. 5, 37-45.

- Ocak, I., Bilgin, N. 2010. Comparative studies on the performance of a roadheader, impact hammer and drilling and blasting method in the excavation of metro station tunnels in Istanbul. *Tunnelling and Underground Space Technology*. 25, 181–187.
- Ocak, I. 2008. Comparison of Machine Utilization Time and Performance for Roadheader and Impact Hammer in Kadikoy-Kartal Metro Tunnels (Istanbul). 8th International Multidisciplinary Scientific GeoConference SGEM 2008. 1-4 July, Bulgaria, pp.269-276.
- Rostami, J., Ozdemir, L., Neil, D.M. 1994. Performance prediction: A key issue in mechanical hard rock mining. *Mining Engineering*. 11, 1263-1267.
- Thuro, K., Plinninger, R.J. 1999. Roadheader excavation performance - geological and geotechnical influences. The 9th ISRM Congress, Theme 3: Rock dynamics and tectonophysics / Rock cutting and drilling, Paris, pp. 1241–1244.
- Tumac, D., Bilgin, N., Feridunoglu, C., Ergin, H., 2007. Estimation of rock cuttability from shore hardness and compressive strength properties. *Rock Mechanics and Rock Engineering*. 40 (5), 477–490.

